



Changes in the impacts of ship emissions on PM_{2.5} and its components in China under the staged fuel oil policies

Guangyuan Yu^{1,2}, Yan Zhang^{1,3,4*}, Qian Wang², Zimin Han¹, Shenglan Jiang¹, Fan Yang⁵, Xin Yang⁶, and Cheng Huang^{2*}

5 ¹Shanghai Key Laboratory of Atmospheric Particle Pollution and Prevention (LAP³), National Observations and Research Station for Wetland Ecosystems of the Yangtze Estuary, Department of Environmental Science and Engineering, Fudan University, Shanghai 200438, China

²Shanghai Environmental Monitoring Center (SEMC), Shanghai 200235, China

³Shanghai Institute of Eco Chongming (SIEC), Shanghai 200062, China

10 ⁴MOE laboratory for National Development and Intelligent Governance, Shanghai institute for energy and carbon neutrality strategy, IRDR ICoE on Risk Interconnectivity and Governance on Weather/Climate Extremes Impact and Public Health, Fudan University, Shanghai 200433, China

⁵Pudong New Area Environmental Monitoring Station, Shanghai 200135, China

15 ⁶Shenzhen Key Laboratory of Precision Measurement and Early Warning Technology for Urban Environmental Health Risks, School of Environmental Science and Engineering, Southern University of Science and Technology, Shenzhen 518055, China

Correspondence to: Yan Zhang (yan_zhang@fudan.edu.cn) and Cheng Huang (huangc@saes.sh.cn)

Abstract. The issue of air pollution caused by ship emissions is becoming prominent with the increasing global shipping activities. China has carried out staged fuel oil policies in the past few years to meet the requirements of the global low sulfur regulation by the International Marine Organization (IMO), called the IMO Regulation. However, the impacts of ship emissions on air quality in China after 2020 are not sufficiently understood. This study firstly updated the ship emission inventory including PM_{2.5} components based on field and on-board measurements under the staged fuel oil policies. Then, the impacts of ship emissions on PM_{2.5} as well as its gas precursors and primary and secondary components in China from 2017 to 2021 have been revealed by using the Weather Research and Forecasting (WRF) model and the Community Multi-scale Air Quality (CMAQ) model. We found that ship emissions increased the PM_{2.5} concentrations up to 3.8 µg m⁻³ in 2017 and 2.6 µg m⁻³ in 2021 along China's coastal area. The areas with high concentration levels widely distributed over the offshore waters in 2017, and shrunk to some parts of China's coast in 2021. The contributions of ship emissions to the PM_{2.5} concentrations over China's main port cities ranged from 3.0% to 17.4% in 2017 and 2.5% to 10.3% in 2021. Our findings suggest that it is important to consider both transport pathways and formation mechanisms of secondary aerosols to combat the PM_{2.5} pollution caused by shipping in different regions.



1 Introduction

Shipping is the backbone of global trade and transports more than 80% of global goods. The global shipping activities increased by ~20% in the past decade, and continues to grow at a rate of ~2% per year in the coming years (UNCTAD, 2023). Meanwhile, heavy fuel oil (HFO) is the most widely used type of fuels for marine vessels. The combustion of HFO can release remarkably higher amounts of sulfur oxides (SO_x), particulate matter (PM), and trace elements compared to the combustion of lighter oils (Agrawal et al., 2008a; Moldanová et al., 2013; Zhang et al., 2019b). Due to the increasing shipping activities and the low quality of fuel oils, shipping is becoming an important source of air pollution, especially in coastal areas and ports with dense traffic (Dalsøren et al., 2009; Eyring et al., 2010). It is reported that international vessels emitted 9600 kt (kilotons) SO_x, 17100 kt NO_x (nitrogen oxides), and 1351 kt PM_{2.5} (PM with a diameter of less than 2.5 μm) in 2018 (IMO, 2021). In Europe, the maritime transport sector produced 24% of all NO_x emissions, 24% of all SO_x emissions, and 9% of all PM_{2.5} emissions in 2018, affecting ~40% of Europeans living within 50 km of the sea (EMSA and EEA, 2021). In 2022, China held a national port cargo throughput of 15.68 billion tons, and was home to eight of the top ten ports for cargo throughput and seven of the top ten ports for container throughput worldwide (Ministry of Transport of the People's Republic of China, 2023). Tracking ship emissions and their environmental impacts in China is of great significance.

Exposure to high levels of PM_{2.5} can increase health problems like respiratory and cardiovascular diseases. The World Health Organization (WHO) Global Air Quality Guidelines 2021 recommend that annual mean concentrations of PM_{2.5} should not exceed 5 μg/m³ (WHO, 2021). Studies using chemical transport models (CTMs) have been conducted to simulate the impact of ship emissions on PM_{2.5} in the regions with heavy ship traffic. In China, ship emissions increased the annual averaged PM_{2.5} concentrations up to 5.2 μg m⁻³ in 2015, surpassing the limit value supposed by the WHO. In Europe and North America, the increase in PM_{2.5} concentrations due to shipping is generally less than 2 μg m⁻³; however, its relative contribution is significant, reaching 25%–50% along main shipping routes and 12%–15% in coastal areas (Aksoyoglu et al., 2016; Tang et al., 2020; Fink et al., 2023a; Golbazi and Archer, 2023). Based on observation, the impact of ship emissions on PM can also be calculated by using source apportionment methods like receptor models. In China, our previous studies show that ship emissions contribute 1.96 μg m⁻³ (4.23%) to the ambient PM_{2.5} concentration at port, while 0.4–3.1 μg



m^{-3} (1.3%–8.8%) for downtown Shanghai (Zhao et al., 2013; Yu et al., 2021); the fraction of shipping-related particles is 1%–10% in port cities (Liu et al., 2017b; Wang et al., 2019; Zhang et al., 2019a; Zhai et al., 2023). Ship emissions contribute to annual mean concentrations of $\text{PM}_{2.5}$ with 1%–14% in
65 European coastal areas and 3%–9% in American coastal areas (Agrawal et al., 2009; Viana et al., 2014; Kotchenruther, 2015; Anastasopoulos et al., 2021).

Shipping-related PM is comprised of primary particles and secondary products. Ships primarily emit organic carbon (OC), elemental carbon (EC), sulfate, metallic elements, etc., among which OC and sulfate are the main components of primary PM from ships burning HFO (Agrawal et al., 2008b; Lack et al., 2009; Agrawal et al., 2010; Huang et al., 2018a; Yang et al., 2022; Karjalainen et al., 2022). Vanadium (V), nickel (Ni), and the V/Ni ratio are the mostly used tracers of ship emissions (Agrawal et al., 2009; Moldanová et al., 2009; Celo et al., 2015; Corbin et al., 2018; Yu et al., 2021). Calculating the emissions, the concentrations, and the deposition fluxes of V and Ni from shipping can help better understanding their geochemical cycles. In comparison, sulfate, nitrate, and ammonium (SNA) dominate
75 the shipping-related PM with its proportion even exceeding 90% based on modeling research (Lv et al., 2018; Jonson et al., 2020; Fink et al., 2023a; Jang et al., 2023).

Studies have demonstrated that using desulfurized fuel oils can significantly reduce the emissions of various air pollutants such as SO_x , PM, OC, heavy metals, and polycyclic aromatic hydrocarbons (PAHs) (Tao et al., 2013; Zetterdahl et al., 2016; Kotchenruther, 2017; Spada et al., 2018; Huang et al., 2018a).
80 To combat the air pollution caused by ship emissions, four Emission Control Areas (ECAs) have been established in Europe and North America since 2011. The sulfur limits for fuel in the ECAs was restricted to 0.10% m/m after 1 January 2015. Besides, the Tier III entered into force on 1 January 2016 in the ECAs of North America and on 1 January 2021 in the ECA areas of Europe. However, the regulations in China are significantly lagging behind those in North America and Europe. Ships berthing at the ports in
85 the China's Domestic Control Areas (DECAs) were required to use fuel with a sulfur content no more than 0.50% (low sulfur fuel oil, LSFO hereafter) after 1 January 2017, which is called the DECA 1.0 period. All ships within 12 nm (nautical miles) from the coastline must use LSFO after 1 January 2019, which is referred to as the DECA 2.0 period (Liu et al., 2018a; Wang et al., 2021). The inland emission control areas covering the Yangtze River, the Xijiang River, and the Pearl River went into effect after 1
90 January 2019 where coastal vessels were required to combust LSFO; both coastal and international vessels must use fuel with a sulfur limit of 0.10% called ultra-low sulfur fuel oil (ULSFO) after 1 January



2020. The rapid transition of China's control measures is to meet the global fuel sulfur limit of 0.50% (reduced from 3.50%) from 1 January 2020 mandated by the IMO (the IMO Regulation). For the NO_x emission control, newly built ships in China follows the IMO Tier II standard from 2011. The staged sulfur regulations are expected to effectively alleviate the air pollution from shipping in China. However, there are very few studies on the impacts of ship emissions on air quality after the implementation of the IMO Regulation based on actual shipping activity data and CTMs (Zhai et al., 2023; Feng et al., 2023). For instance, the simulation years of the recently published studies from China, Europe, and North America are generally before the IMO Regulation (Fink et al., 2023b; Fu et al., 2023; Golbazi and Archer, 2023). There is relatively little research on simulating the specific composition of shipping-related PM. The impacts of meteorology and chemical mechanisms on the PM_{2.5} pollution caused by shipping in China are not fully understood. In addition, it has been observed that the concentrations of V and Ni from shipping experienced a markedly and stepwise decrease in China's largest port city from 2017 to 2020 in our previous study. The latest emission inventories of V and Ni from shipping are still not earlier than 2017, and need updating until after 2020 (Zhao et al., 2021; Jiang et al., 2024).

In this study, we updated the ship emission inventory based on the data from the Automatic Identification System (AIS), and simulated the impacts on PM_{2.5} in China as well as its gas precursors (SO₂ and NO₂) and components from 2017 to 2021 by using the Weather Research and Forecasting (WRF) model and the Community Multi-scale Air Quality (CMAQ) model. The emissions of V and Ni from shipping were constrained by the field observational data from our previous study and the results of on-board emission measurements. Based on the simulation results, the spatiotemporal patterns of shipping-related PM_{2.5} as well as trace elements (V and Ni), secondary inorganic aerosols, and organic aerosols were obtained. Meanwhile, the interannual and seasonal variations of the impacts were investigated. Then, we focused on the changes in the impacts due to the implementation of the IMO Regulation at the port city level. Besides, the roles of the meteorological factors in affecting the seasonal and diurnal patterns of primary PM from shipping over the port cities were discussed.



2 Methods

2.1 Setup of the WRF/CMAQ

120 We utilized the CMAQ version 5.4 to simulate the pollutant concentrations, and the WRF version 4.1.1
to provide the meteorological input fields for the CMAQ. The WRF physics scheme configuration
included the Yonsei University (YSU) for the planetary boundary layer (PBL) scheme, the Noah land
surface scheme, the Thompson microphysics scheme, the rapid radiative transfer model for general
circulation models (RRTMG) for short and long wave schemes, and the Kain-Fritsch cumulus scheme
125 for cumulus parameterization. 40 vertical layers were setup with the model top pressure at 50 hPa, among
which 12 layers were distributed within 1.6 km above the surface. The surface layer thickness was ~50
m. The WRF model was driven by the European Centre for Medium-Range Weather Forecasts (ECMWF)
Reanalysis v5 (ERA5) at hourly temporal and $0.25^\circ \times 0.25^\circ$ spatial resolution (Hersbach et al., 2023). To
reduce the errors, monthly WRF simulations were divided into six runs, each of which included 12-h
130 spin-up time. Two nested domain simulations were operated with horizontal resolutions of $27 \text{ km} \times 27$
 km (d01) and $9 \text{ km} \times 9 \text{ km}$ (d02) encompassing East Asia and eastern China, respectively. In the CMAQ
model, two grids on each WRF lateral boundary were removed, and thus there were 161×174 and 233
 $\times 215$ grids in d01 and d02, respectively. Figure 1 shows the nested domains configured in the CMAQ
as well as the coastal emission control area (CECA) of China covering all the marine waters within 12
135 nm beyond the territorial baselines.

The CMAQ model was configured to the gas-phase mechanism of Carbon Bond 6 revision 5 (CB6r5)
and the aerosol module of AERO7. By modifying the aerosol module and the in-line dust module, two
trace elements, V and Ni, were added into the CMAQ as inert aerosol components which only participate
in atmospheric physical processes such as diffusion, advection, and deposition. Detailed information on
140 the code modification can be found in our previous study (Jiang et al., 2024). The initial and boundary
conditions for d01 originated from the seasonal average hemispheric CMAQ output from the Community
Modeling and Analysis System (CMAS) data repository, while those for d02 were derived from the
output data of d01. For the analysis of seasonal variations, the simulations were conducted for January,
April, July, and October of 2017 and 2021, representing winter, spring, summer, and autumn, respectively.
145 The annual average was equal to the average of four representative months. To study the impacts under
staged fuel oil policies and save computing resources meanwhile, the simulations were operated for each

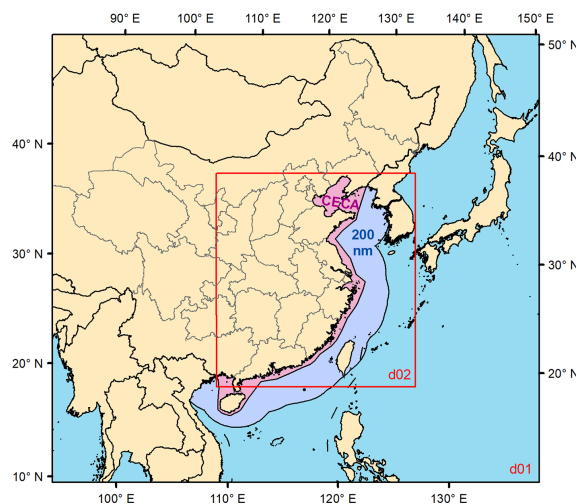


Figure 1. Map of the nested domains configured in the CMAQ. The coastal emission control area (CECA) of China is colored in pink. The border of the area within 200 nautical miles (nm) from the coastline of Chinese Mainland is outlined.

150

Table 1. Details of the WRF/CMAQ configuration.

Simulation period	January, April, July, and October of 2017 and 2021; April of 2018–2020
Grid resolution	27 km × 27 km (d01), 9 km × 9 km (d02)
Vertical layers	40
Surface layer thickness	50 m
Top of model	50 hPa
WRF version 4.1.1	
Grid size	165 (south to north) × 178 (west to east) (d01); 237 × 219 (d02)
Initial/boundary conditions	ERA5 (ECMWF Reanalysis v5), hourly, 0.25° × 0.25°
Microphysics scheme	Thompson
Land surface model	Noah
Planetary boundary layer scheme	YSU (Yonsei University), topo_wind = 2
Cumulus scheme	Kain-Fritsch
Shortwave radiation	RRTMG (Rapid Radiative Transfer Model for General circulation models)
Longwave radiation	RRTMG
Spin-up time	12 h
Number of days per run	6.5*
CMAQ version 5.4	
Grid size	161 × 174 (d01); 233 × 215 (d02)
Initial/boundary conditions	EPA 2017–2018 (d01); output of d01 run (d02)
Gas-phase mechanism	Carbon Bond 6, revision 5 (CB6r5)
Aerosol module	AERO7
Spin-up time	5 days
Number of days per run	36 for January, July, and October; 35 for April

*For WRF, the last run of April is an exception with the time length of 5.5 days.

155 April from 2017 to 2021 based on our previous finding that the impacts of ship emissions in China's coastal areas usually peak in spring (Yu et al., 2021). The spin-up time of each simulation was 5 days. Detailed information on the WRF/CMAQ configuration can be seen in Table 1. The impacts of ship



emissions were extracted based on the zero-out method, i.e., two runs with and without ship emissions, named the base run and the exship run respectively in this study.

2.2 Emission data

160 2.2.1 Ship emissions

A bottom-up ship emission model based on the AIS data was used to calculate the emission inventories of SO₂ (sulfur dioxide), NO_x, CO (carbon monoxide), NMVOCs (nonmethane volatile organic compounds), PM₁₀ (PM with a diameter less than 10 μm), PM_{2.5}, NH₃ (ammonia), V, and Ni. Detailed information on the setup of the ship emission model and the low load adjustment multipliers for main engine emission factors (EFs) can be found in the previous studies (Fan et al., 2016; Feng et al., 2019). In the ship emission model, the power-based EFs under the staged fuel oil policies are categorized by engine type (Table S1).

During the DECA 1.0 period (2017–2018), we adopted the EFs of various species from Fan et al. (2016) and the fourth IMO Greenhouse Gas (GHG) study. The default setting for main engines (MEs) including slow-speed diesel (SSD) and medium-speed diesel (MSD) engines usually installed for large vessels was using high sulfur fuel oil (HSFO) with a sulfur content of ~2.7%. A high-speed diesel engine as a main engine (ME_HSD) generally used marine diesel oil (MDO) or marine gas oil (MGO) with a sulfur content of ~0.1%. An auxiliary engine (AE) was assumed to use LSFO with a sulfur content of ~0.5%.

During the DECA 2.0 period (2019), the settings remained the same as those during the DECA 1.0 period in the marine areas outside the CECA. In the CECA, the scenario of EF setting for MEs of large vessels was using LSFO. For the AE, considering that LSFO is often used by sea-going vessels in addition to ULSFO, we took the mean values of the EFs for LSFO and ULSFO.

After the implementation of the IMO Regulation, the settings in all marine areas followed those in the CECA during the DECA 2.0 period. Over land areas, for the sea-going vessels, the EFs of SO₂ and PM for ME were scaled by a factor of 0.2 and 0.26, and 0.315 and 0.391 for AE, respectively, which is due to the implementation of the inland river emission control areas. The EFs of V and Ni for ships navigating in inland waters were lowered by a factor of 10 for the ME due to the nonlinearity between the contents of sulfur and trace elements.



185 In terms of the EFs of V and Ni for marine vessels during the DECA 1.0 period, we used the values reported in the literature listed in Table S2. These values during the DECA 2.0 and after 2020 were reduced corresponding to the change ratios reported in our previous study (Yu et al., 2021). The emission inventories of V and Ni were validated through comparison between simulation results and observational data in Shanghai.

190 The mapping of PM_{2.5} components from shipping to the AERO7 species is shown in Table S3. The mass fractions before the IMO Regulation (2017–2019) and after 2020 were referenced from Huang et al. (2018a) and Yang et al. (2022), respectively. The convert factors of NMVOCs emissions from shipping to lumped species in the CB6 mechanism were based on the median VOC profiles from the literature (Table S4) (Agrawal et al., 2008a; Huang et al., 2018b; Zhang et al., 2024). The initial height of ship
195 emissions considering plume rise and diffusion is basically with the range of 20–100 m (Chosson et al., 2008; He et al., 2021; Badeke et al., 2022; Lansø et al., 2023). We allocated 20% of the sea-going vessel emissions to the surface layer (0–50 m) and 80% to the second layer (50–109 m), while all the inland ship emissions were assigned in the surface layer (Table S5).

2.2.2 Land-based emissions

200 For land-based anthropogenic emissions, we used the Multiresolution Emission Inventory for China (MEIC) in 2017–2020 for mainland China and the MIX emission data in 2010 for East Asia excluding mainland China (Li et al., 2017; Zheng et al., 2021). The NH₃ emissions in the MEIC were replaced by the PKU-NH₃ inventory in 2017 (Kang et al., 2016). For natural sources, we used the CAMS-GLOB-BIO v3.1 for monthly global biogenic VOC (BVOC) emissions in 2017–2021 and the biogenic emissions
205 inventory from urban green spaces in China (OUC-BUGS) in 2017–2019 (Sindelarova et al., 2021; Ma et al., 2022). The MEIC, MIX, PKU-NH₃, and OUC-BUGS inventories were downloaded from the website (<http://meicmodel.org.cn/>). The grid resolutions of MEIC/MIX, BVOC, UBVOC, and PKU-NH₃ are 0.25°, 0.25°, 27 km, and 0.1°, respectively. The PM_{2.5} profiles in Liu et al. (2017a) were used to convert PM_{2.5} from non-shipping emissions to the AERO7 species. We multiplied the PM_{2.5} emissions
210 from the MEIC/MIX by the V and Ni fractions in PM_{2.5} in China by source to obtain the V and Ni emissions from anthropogenic sources excluding shipping (Liu et al., 2018b). The source-specific vertical profiles for industrial, power, residential, and land-based transportation emissions in Table S5 were referenced from Zheng et al. (2019).



2.3 Observational data and evaluation of simulation results

215 The observational data from the national meteorological stations and the national air quality
monitoring stations listed in Table S6 were used to evaluate the simulation results. The hourly
meteorological data were downloaded from the website (<http://data.cma.cn>), and the hourly air quality
data were obtained from China National Environmental Monitoring Center (<https://air.cnemc.cn:18014>).
To evaluate the model performance for $PM_{2.5}$ in coastal areas, 21 port cities along the coast of China were
220 selected as representatives. They rank among the top 20 in terms of cargo or container throughput
nationwide and distribute on the coasts of the Bohai Rim (Dalian, Yingkou, Caofeidian, Binhai of Tianjin,
and Yantai), the Yellow Sea (Qingdao, Rizhao, and Lianyungang), the Yangtze River Delta (Shanghai,
Ningbo, Zhoushan, Hangzhou, Nantong, Zhangjiagang, and Nanjing), the Pearl River Delta (Shenzhen,
Guangzhou, and Zhuhai), and the Beibu Gulf (Qinzhou) as well as on the west coast of the Taiwan Strait
225 (Fuzhou and Xiamen). The simulated concentrations in the surface layer were used to compare with the
observational data.

We used the hourly observational data from the Pudong site of Shanghai to evaluate the model
performance of the tracers of ship emissions (V and Ni) and the secondary inorganic aerosols (SO_4^{2-} ,
 NO_3^- , and NH_4^+). The metallic elements and the ions were measured by the Model Xact 625 (Cooper
230 Environmental Services, LLT, OR, USA) and the MARGA (Model ADI 2080, Applikon Analytical B. V.
Corp., The Netherlands), respectively. Detailed information on the location of the monitoring site and the
online instruments can be found elsewhere (Yu et al., 2021).

To quantify the model performance, the Spearman's correlation coefficient (r) and the normalized
mean bias (NMB) were calculated for 2-m temperature, wind speed, SO_2 , NO_2 , O_3 (ozone), and $PM_{2.5}$ at
235 each monitoring station listed in Table A1. The index of agreement (IoA) and the root mean square error
(RMSE) were also calculated for the $PM_{2.5}$ component monitoring at the Pudong site.

3 Results and discussion

3.1 Changes in ship emissions under the staged fuel oil policies

The emissions of SO_2 , NO_x , CO, NMVOCs, $PM_{2.5}$, V, and Ni from shipping in the CECA and inland
240 waters of China from 2017 to 2021 were calculated based on the method introduced in Sect. 2.2.1 (Table



2) NO_x is the major pollutant from shipping, and the nitrogen control policy has not been changed nationwide in the study period. Hence, the amount of NO_x emission can be regarded as a proxy of ship traffic volume. As mentioned in Sect. 1, the variations of emissions in each April from 2017 to 2021 were used to represent the interannual variations. In the CECA and inland waters of China, the NO_x emissions from shipping gradually increased from 2017 to 2020, with the largest increase (37.1%) from 2017 to 2018, and then slightly decreased in 2021. Due to the increase in ship activities, the NO_x emissions from shipping increased by 51.8% from 2017 to 2021. Figure S1 depicts the spatial distribution of NO_x emissions from shipping in each April from 2017 to 2021 with high values along the major shipping routes of coastal China, the Yangtze River and its main branches, and the Pearl River. In April 2019, the higher emission intensity on the main route along the southeast coast of China was due to the bypass behavior that ships tend to navigate outside the CECA. For the seasonal patterns, in 2017, the NO_x emissions from shipping were higher in April (114.1 kt) and October (112.1 kt), smaller in July (101.6 kt) due to the fishing ban, and reached the lowest value in January (89.9 kt) which includes the Spring Festival. However, in 2021, the lowest value (128.9 kt) occurred in July, while January exhibited relatively high NO_x emissions (169.2 kt) as the Spring Festival was in February.

By contrast, in the same area, the monthly average SO_2 ($\text{PM}_{2.5}$) emissions from shipping of January, April, July, and October decreased by 68.4% (32.8%) from 2017 to 2021 due to the implementation of the IMO Regulation and China's inland sulfur regulation. The monthly average $\text{PM}_{2.5}$ emissions reduced from 7.6 kt in 2017 to 5.1 kt in 2021. In addition, the monthly average V emissions from shipping experienced a dramatic drop (by 90.8%) from 118.8 t in 2017 to 43.9 t in 2021. The monthly average Ni emissions decreased from 11.0 t in 2017 to 24.1 t in 2021, with a reduction of 42.0%. The average V/Ni ratio decreased from 2.86 in 2017 to 0.46 in 2021. Figure S2 (Figure S3) shows the interannual variations of V (Ni) emissions from shipping and anthropogenic sources excluding shipping. It can be clearly seen that higher V and Ni emissions transferred from nearshore waters to the outer border of the CECA in 2019.

Table S7 shows the contributions of ship emissions to the total anthropogenic emissions in China's 200-nm zone and coastal provinces (coastal areas hereafter). The staged low sulfur policies since 2017 significantly reduced the SO_2 , V, and Ni emissions, and their reduction rates were larger than those from land-based anthropogenic sources, especially for V. The contributions of ship emissions to the total SO_2 , V, and Ni emissions in the coastal areas decreased from 13.9%, 89.2%, and 55.5% in 2017 to 7.7%,



56.0%, and 53.8% in 2021, respectively. The contribution of ship emissions to the total PM_{2.5} emissions in the coastal areas remained at 4.0%. However, the share of NO_x emissions from shipping increased from 13.2% in 2017 to 21.2% in 2021 due to the increase in shipping activities and the reduction in emissions from land-based sources.

275

Table 2. Time variation of emissions of SO₂, NO_x, CO, NMVOCs, PM_{2.5}, V, and Ni from shipping in the coastal emission control area (CECA) and inland waters of China.

	SO ₂ (kt)	NO _x (kt)	CO (kt)	NMVOCs (kt)	PM _{2.5} (kt)	V (t)	Ni (t)
January 2017	35.3	89.9	4.2	4.6	6.5	102.1	35.7
April 2017	44.4	114.1	5.4	6.0	8.3	130.7	45.7
July 2017	40.3	101.6	4.6	5.1	7.2	115.0	40.2
October 2017	43.5	112.1	5.3	5.9	8.2	127.4	44.7
April 2018	63.2	156.4	7.3	8.1	11.5	185.9	64.7
April 2019	13.2	166.7	8.1	8.9	5.3	51.1	29.1
April 2020	14.3	170.9	8.1	9.0	5.7	15.3	32.0
January 2021	13.8	169.2	8.2	8.6	5.4	12.1	26.4
April 2021	13.9	164.8	8.0	8.3	5.4	11.8	25.9
July 2021	10.4	128.9	6.1	6.2	4.0	8.2	18.3
October 2021	13.6	171.0	8.4	8.9	5.5	11.7	25.7
2017 average per month	40.9	104.4	4.9	5.4	7.6	118.8	41.6
2021 average per month	12.9	158.5	7.7	8.0	5.1	11.0	24.1

Note: Average per month equals the average of emissions during January, April, July, and October.

3.2 Model performance

280 Uncertainties in simulation results of air quality can be caused by multiple factors such as the accuracy
of meteorological inputs, uncertainties in emission inventories, and the simplification of mechanisms in
the model. For meteorological elements, as shown in Table S8, the model can outstandingly reproduce
the 2-m temperature in each city during the 11 simulated months from 2017 to 2021. Except for Qinzhou
($r = 0.88$), the r values of the other cities were all above 0.9, and over 0.95 for most cities. The
285 performance for relative humidity was slightly inferior to that of temperature, with correlations ranging
from 0.7 to 0.8 in most cities. Except for Dalian (NMB = 2.4%), all other cities show negative biases,
which was caused by the underestimation of nighttime radiation cooling. For the 10-m wind speed,
overestimation was found in most cities especially megacities such as Shanghai (NMB = 95.5%) and
Shenzhen (NMB = 72.2%). The WRF model with a resolution of 9 km can generally reproduce the
290 average wind direction at a station level which is significantly affected by local topography.

For the concentration of pollutants, the simulation results from the base runs were used to evaluate the
model performance of the CMAQ model. As shown in Table S9, large biases of over $\pm 50\%$ of the



concentration levels of SO₂ and NO₂ derived from the CMAQ were found in three megacities including Shanghai, Shenzhen, and Beijing with positive biases, and in Qinzhou with negative biases. These biases
295 were caused by the uncertainties in local emissions of the MEIC inventory. In general, the performance for the daily maximum 8-h average (MDA8) O₃ concentrations in the coastal cities showed the patterns of underestimation in Zhejiang province and to its north and overestimation in Fujian province and to its south, corresponding to the biases of NO₂ concentration. It is noted that the PM_{2.5} concentrations were underestimated in all of the 21 port cities that we concerned, with an average NMB of -31.0% (Fig. 2a),
300 which was mainly attributed to the underestimation of secondary aerosols. For example, the NMB values of the concentrations of sulfate, nitrate, and ammonium in Shanghai reached -15.4%, -54.6%, and -21.8% respectively in the entire simulation periods (Table S10). Multiple causes can result in the underestimation of secondary aerosols especially nitrate such as lack of chemical mechanisms, underestimation of daytime O₃ and nighttime relative humidity, as well as overestimation of wind speed
305 (Sun et al., 2022; Xie et al., 2022). The negative biases were larger in spring, which was likely due to insufficient consideration of heterogeneous reactions like reactions on the surface of mineral dust in the CMAQ model. Nevertheless, the model can reproduce the temporal variation of mean PM_{2.5} concentrations, with a correlation of $r = 0.80$.

For the shipping-related PM_{2.5} concentrations in the concerned port cities, the mean value during the
310 simulation periods was 1.6 µg m⁻³ (Fig. 2b). The hourly mean shipping-related PM_{2.5} peaked on the early morning of 27 July 2017 (local time, hereafter) with a concentration of 10.4 µg m⁻³, while the minimum value of -0.9 µg m⁻³ occurred on the morning of 2 January 2021. Shipping is an emission sector releasing large amounts of NO_x which can participate in complex non-linear chemistry. The limitation of chemical mechanisms in the model could lead to systematic uncertainties. Ship-emitted NO_x significantly
315 consumes atmospheric oxidants such as O₃ and various radicals (OH, HO₂, RO₂, etc.) in areas controlled by the VOC-limited regime. The potential reduction of these oxidants can inhibit the second aerosol formation, which is the major reason for the negative simulated values of PM_{2.5} related to ship emissions.

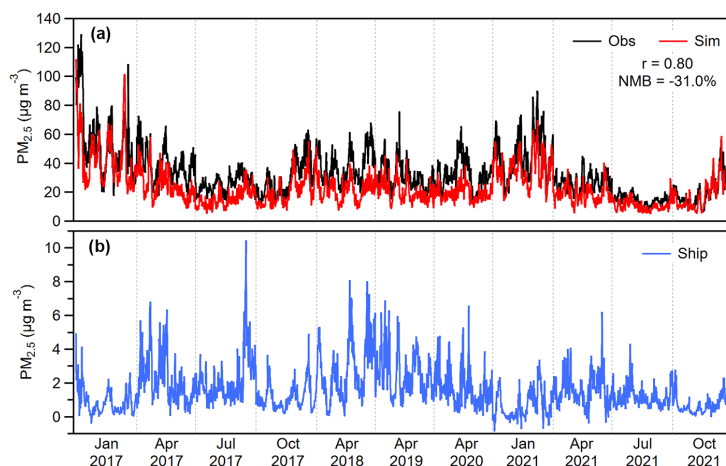


Figure 2. Time series of hourly mean $PM_{2.5}$ concentrations during the simulation periods, averaged for the representative port cities of China: **(a)** observational data (Obs) and simulated results of base runs (Sim), as well as **(b)** simulated shipping-related $PM_{2.5}$.

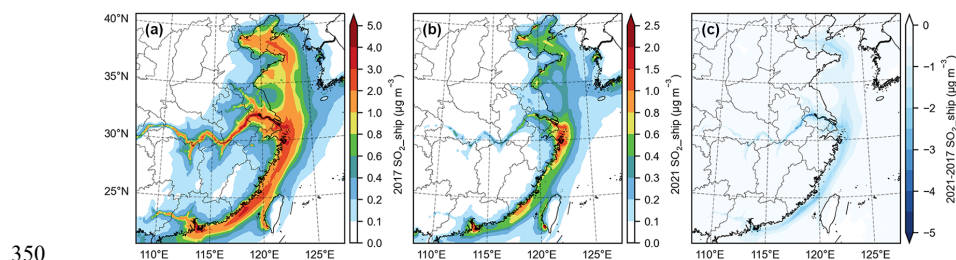
Regarding the tracers of ship emissions, as shown in Table S11, the simulated results of the monthly mean concentrations of V and Ni, as well as the Ni/V ratios are acceptable, thus the emission inventories of V and Ni established in this study being applicable. The model successfully reproduced the changing impacts of fuel oil policies on V and Ni. For the uncertainties, the model tended to overestimate the concentrations of the two metals in winter, such as overestimating the concentrations of V and Ni in January 2017 by 41% and 30%, respectively. The pattern in July 2021 was underestimating both V and Ni concentrations by 38%. These results can be brought by uncertainties in the simulation of diffusion conditions. The CMAQ model was fed by monthly ship emissions, and the high-frequency ship traffic data was smoothed, resulting the relatively weak temporal correlation between observational data and simulation results with hourly resolution. In addition, the uncertainties in meteorology can also affect the simulation of the transport process of ship emissions to urban areas. Nevertheless, the model can characterize the diurnal variation patterns of V (Fig. S4), with higher values during the nighttime and lower values during the daytime. The daily variations of simulation results were more pronounced than those based on observation, which was due to the overestimation of the diurnal cycle of the PBLH using the YSU PBL scheme (Du et al., 2020).

3.3 Spatiotemporal patterns of the shipping-related gas precursors of $PM_{2.5}$

SO_2 and NO_2 are the key gas precursors of secondary aerosols and the important pollutants from



shipping, and thus their spatiotemporal patterns are of interest. Figure 3 depicts the impacts of ship
 340 emissions on the SO₂ concentration during the DECA 1.0 period (represented by 2017) and after the
 implementation of the IMO Regulation (represented by 2021). In 2017, the spatial pattern of the SO₂
 concentration from shipping performed high values along the main routes with the maximum value of
 6.1 μg m⁻³ (in a grid cell level) in the Yangtze River Estuary (YRE), and a decreasing trend toward both
 sides (Fig. 3a). In 2021, the hotspots in China's coastal areas were located to the east of Shanghai and
 345 Zhejiang, to the southeast of Fujian, and in the Pearl River Estuary (PRE), with the highest value of 2.5
 μg m⁻³ (Fig. 3b). With a remarkable decrease in fuel sulfur content (FSC) globally, the SO₂ concentration
 from shipping reduced in all simulated areas (Fig. 3c). The largest reduction was observed in the lower
 reaches of the Yangtze River reaching 5.2 μg m⁻³ due to the fuel type shift to the ULSFO.



350 **Figure 3.** Impacts of ship emissions on the SO₂ concentrations (SO₂_ship) in (a) 2017 and (b) 2021, as well as its
 (c) absolute change from 2017 to 2021. The annual average equals the average of January, April, July, and October
 here and hereafter.

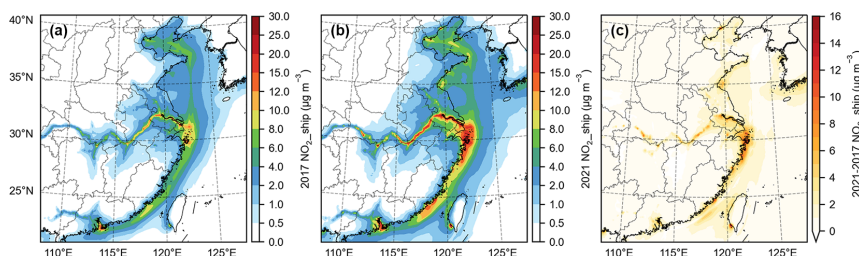
As SO₂ is a typical primary pollutant emitted by ships, it was selected to analyze the factors affecting
 355 the seasonal and interannual patterns such as emission intensity and meteorological conditions. With
 respect to the seasonal patterns, the highest SO₂ concentrations from shipping in most regions of China
 occurred in spring when the prevailing wind was weak and generally blew onshore in the areas with high
 ship emissions (Fig. S5). Meanwhile, the ship emissions in spring were in a high level with ~8% higher
 than the annual average. Hence, we selected April as the representative month for the analysis of
 360 interannual variations. In winter, the concentrations on the land showed higher values due to the weak
 diffusion conditions. In the offshore areas, the concentrations in winter were not high as those in spring,
 which was caused by the significant winter monsoon. In summer, despite the better diffusion conditions,
 the concentrations in the areas with dense ship emissions were only second to those in spring in 2017.
 However, the concentrations shared relatively low levels in summer and autumn in 2021. This difference



365 can be attributed to the direction and the intensity of the summer monsoon. In the summer of 2021, the strong southeasterly wind was in favor of the diffusion of ship emissions. Although the ship emissions in autumn were comparable to those in spring, the concentrations in autumn were much lower than those in spring in marine areas, which was resulted from the northeasterly prevailing wind diluting the pollutants emitted by ships.

370 Figure S6 shows the variations of the SO₂ concentrations from shipping in each April from 2017 to 2021. The overall concentrations experienced staged reduction with the changes of the fuel oil policies. However, due to large variations in local emissions, the maximum value in each year presented a fluctuating trend with 7.3, 30.1, 7.1, 11.4, and 4.3 μg m⁻³ from 2017 to 2021. The hotspots located in the central part of the coast of Zhejiang in 2018 and 2020 were likely due to the intensive fishing activities.

375 Besides, the simulated wind field patterns in the coastal areas were similar in April of 2017, 2018, 2019, and 2021. However, in April 2020, a stable high-pressure system over the Yellow Sea led to a better horizontal diffusion condition for the emissions on the main routes.



380 **Figure 4.** Impacts of ship emissions on the NO₂ concentrations (NO₂_ship) in (a) 2017 and (b) 2021, as well as its (c) absolute change from 2017 to 2021.

The main source of the ambient NO₂ from shipping is the rapid oxidation of NO in ship plumes, and the high concentrations still fixed on the main routes and ports in the lower reaches of the Yangtze River and the PRE, as well as coastal Shanghai, Zhejiang, and Fujian (Fig. 4). The maximum values in 2017 and 2021 were 17.9 and 26.0 μg m⁻³, respectively. The concentrations increased in most areas from 2017

385 and 2021 were 17.9 and 26.0 μg m⁻³, respectively. The concentrations increased in most areas from 2017 to 2021, and the increase was larger near the ports of Ningbo-Zhoushan in Zhejiang, Quanzhou in Fujian, Gaoxiong in Taiwan, and Tangshan in Hebei with the maximum of 15.4 μg m⁻³. The decrease in SO₂ and the increase in NO₂ were both significant from 2017 to 2021, which is expected to affect the formation pathways of shipping-related secondary aerosols and the composition of shipping-related PM_{2.5}.



390 3.4 Spatiotemporal patterns of shipping-related PM_{2.5} and its components

3.4.1 Fine particulate matter (PM_{2.5})

PM_{2.5} related to ship emissions contains primary and secondary aerosols, and the secondary aerosols lead to the difference in the spatial patterns between the gas precursors and PM_{2.5}. As shown in Fig. 5a, the concentrations of shipping-related PM_{2.5} in 2017 displayed values of over 2 $\mu\text{g m}^{-3}$ along the main routes from the Yellow Sea to coastal Fujian, with the maximum of 3.8 $\mu\text{g m}^{-3}$ near Zhoushan Islands. The areas with concentration over 1 $\mu\text{g m}^{-3}$ covered most of the Yellow and Bohai Seas and extended to the Middle Yangtze River (~1000 km away from the coast). However, the areas with concentration over 1 $\mu\text{g m}^{-3}$ shrunk to the coast and the central Yangtze River Basin in 2021, with the maximum of 2.6 $\mu\text{g m}^{-3}$ in the eastern Shandong Peninsula (Fig. 5b). The areas with shipping-related PM_{2.5} of over 0.1 $\mu\text{g m}^{-3}$ occupied most of the model domain both in 2017 and 2021, which was markedly different from the patterns of SO₂ and NO₂ from shipping. This result is caused by sustained aging processes during the transport of ship-emitted pollutants as well as the longer lifetime of PM compared to SO₂ and NO₂ (Seinfeld and Pandis, 2016). The decrease in the concentration of shipping-related PM_{2.5} showed the largest value of 1.9 $\mu\text{g m}^{-3}$ in the sea area of Zhoushan Islands, while the slight increase within 0.5 $\mu\text{g m}^{-3}$ was found in very small areas in Hunan, Shandong, and Liaoning provinces (Fig. 5c). The result in Lv et al. (2018) showed that the increased PM_{2.5} concentration in China caused by shipping was up to 5.2 $\mu\text{g m}^{-3}$ in 2015. The values in this study were 3.8 $\mu\text{g m}^{-3}$ in 2017 and 2.6 $\mu\text{g m}^{-3}$ in 2021, demonstrating the decreasing trend of the shipping-related PM_{2.5} concentration under the staged fuel oil policies in China.

410 For the relative potential impact of ship emissions on PM_{2.5}, also called the contribution of ship emissions to ambient PM_{2.5}, in 2017, larger values of over 10% distributed along the main routes from the southern Yellow Sea to the northern South China Sea, with the maximum of 21.3% in the Taiwan Strait (Fig. 5d). The distance between the land areas with the relative impact of over 4% and the coast could be up to ~300 km. The relative impact was not less than 1% in the model domain except for northwestern China. Lower values in remote marine areas were related to the contribution of sea salt. In 2021, the relative impact values exceeding 10% were found only along China's southeast coast and in the eastern end of Shandong Peninsula, with the maximum of 16.9% (Fig. 5e). In the areas with high relative impact values mentioned above, the relative impact decreased remarkably, with the largest



420 decrease of -11.0 percentage points (Fig. 5f). However, an increase in the relative impact was observed near the south and east coast of Shandong with the maximum of 3.4%, and small positive changes scattered in China's inland areas. This result may be caused by the increase in nitrate formation related to shipping and the decrease in land-based anthropogenic emissions, which will be discussed in Sect. 3.4.3.

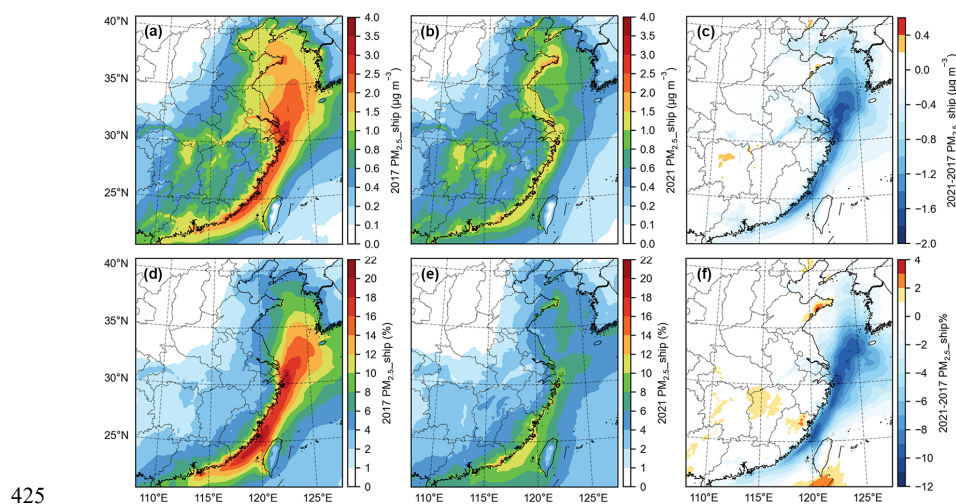


Figure 5. Potential impacts of ship emissions on $PM_{2.5}$ ($PM_{2.5_ship}$): for concentration (in $\mu g m^{-3}$) in (a) 2017 and (b) 2021, as well as (c) the absolute change from 2017 to 2021; and for contribution (in %) in (d) 2017 and (e) 2021, as well as (f) the change of percentage from 2017 to 2021 (in percentage point).

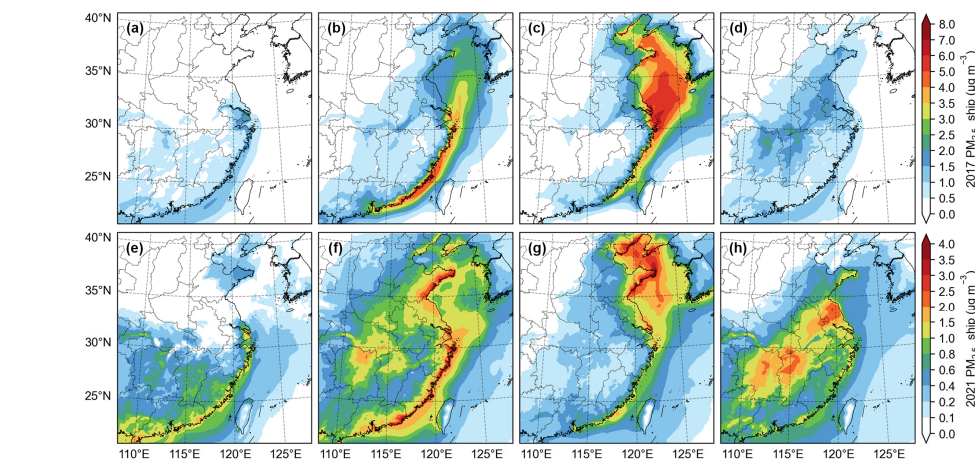


Figure 6. Seasonal patterns of the potential impacts of ship emissions on $PM_{2.5}$ ($PM_{2.5_ship}$) concentrations in (a) January, (b) April, (c) July, and (d) October of 2017; and (e) January, (f) April, (g) July, and (h) October of 2021.



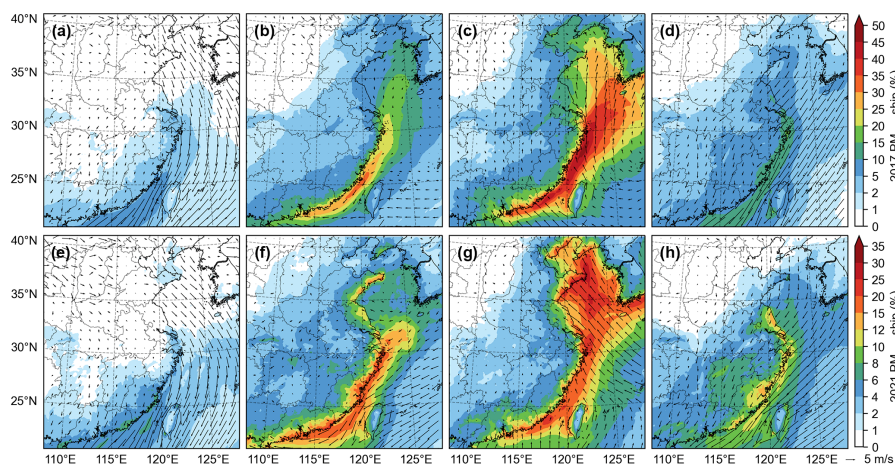
The seasonal patterns of the concentrations of shipping-related PM_{2.5} in 2017 and 2021 were rather different from those of the SO₂ and NO₂ concentrations from shipping (Fig. 6). During the springtime, relatively high shipping-related PM_{2.5} concentration was located along the southeast coast both in 2017
435 and 2021 as well as the coast of Shandong in 2021. The pollutants emitted by ships were prone to accumulate due to the meteorology and experience chemical reactions in coastal areas in spring. Unexpectedly, the hotspots transferred to sea areas in summer, and the maximum values were even higher than those in spring for both years. As the diffusion conditions are better in summer, there should be other factors like secondary organic aerosol (SOA) formation (see Sect. 3.4.4).

440 In autumn, cold air masses from northeastern Asia diluted the gas precursors in coastal areas. The atmosphere over inland areas were in an ammonia-rich condition favoring nitrate formation, and thus relatively high values shifted to inland areas. During the wintertime, the shipping-related PM_{2.5} concentration showed moderate levels in Shanghai both in 2017 and 2021, as well as along the southeastern to southern coast in 2021. It is worth noting that the values in most northern China did not
445 exceed 0.5 µg m⁻³ and even lower than 0.1 µg m⁻³ in some coastal areas, which was very different from the pattern of SO₂ from shipping. Weaker diffusion conditions and lower temperature as well as higher nocturnal humidity led to higher efficiency of secondary aerosol formation. However, NH₃ is sufficiently consumed by SO₂ and NO_x from land-based emissions, and thus the formation of secondary aerosols related to shipping is inhibited, which called the competitive mechanism by land-based sources. As
450 discussed in Sect. 3.3, meteorology is a much more important factor affecting the seasonal patterns of the SO₂ and NO₂ concentrations from shipping compared to emissions. However, the conversion rate of gas precursors is a key factor affecting the seasonal pattern of the concentration of shipping-related PM_{2.5}, while the influence of diffusion conditions is relatively small.

For the relative impact of shipping-related PM_{2.5}, the seasonal pattern generally showed a decreasing
455 trend in summer, spring, autumn, and winter in the model domain, which was mainly due to the impact of the East Asian monsoon on the relative spatial distribution of ship and land-based emissions (Fig. 7). Despite the fact that the concentration of shipping-related PM_{2.5} in coastal areas peaked in spring, the highest relative impact was recorded in summer. In the summer of 2017, the largest relative impact exceeded 50% and 25% over the marine and land areas of the southeastern coastal areas, respectively. In
460 the summer of 2021, the areas with higher absolute and relative impacts of shipping-related PM_{2.5} shifted northward to the Yellow Sea, which was driven by the southeasterly summer monsoon. Among the



concerned port cities, in the summer of 2017, Zhoushan showed the highest value of 37.6%, while the lowest value of 4.8% for Qinzhou. In the summer of 2021, the highest (25.0%) and the lowest values (4.2%) occurred in Zhoushan and Nanjing, respectively. In comparison, the relative impact was much smaller in winter, with the highest value of 5.7% in Ningbo and the lowest value of 0.14% in Caofeidian in the winter of 2017, and the highest value of 6.2% in Fuzhou and the lowest value of 0.04% in Nanjing in the winter of 2021.

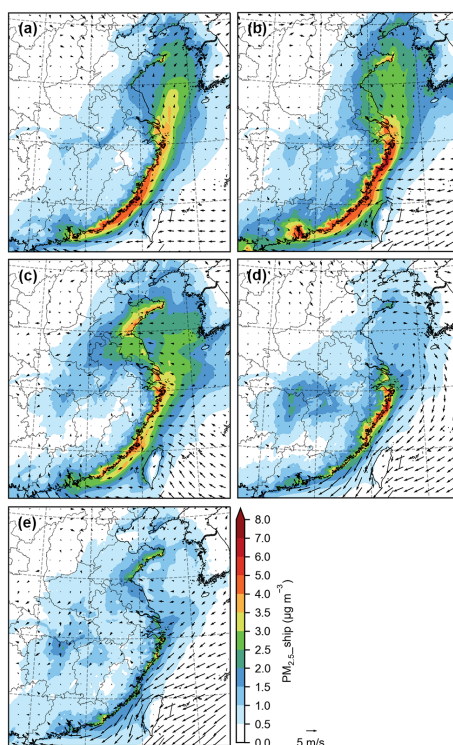


470 **Figure 7.** Seasonal patterns of the potential impacts of ship emissions on PM_{2.5} (PM_{2.5}_ship) for contribution as well as the simulated monthly average wind fields in (a) January, (b) April, (c) July, and (d) October of 2017; and (e) January, (f) April, (g) July, and (h) October of 2021.

Figure 8 shows the spatial patterns of the concentration of shipping-related PM_{2.5} in the spring of 2017–2021. In April 2017, the highest concentration of 7.2 $\mu\text{g m}^{-3}$ was located over the coastal waters of Fujian. In April 2018, the highest concentration rose to 10.4 $\mu\text{g m}^{-3}$; the concentration generally increased in the model domain, especially over the PRE and the coastal waters of Zhejiang, which was due to the increase in shipping activities. In April 2019, high values were closer to the coastline compared to the DECA 1.0 period, and the CECA border was indistinct compared to the pattern of the SO₂ concentration from shipping. This result highlights the crucial role of secondary aerosols in the shipping-related PM_{2.5} in the presence of plenty NH₃ emissions. The highest concentration reduced to 6.5 $\mu\text{g m}^{-3}$, whereas there was an increase along the coast of Shandong due to more secondary aerosol formation. In April 2020, due to the implementation of the IMO Regulation, the concentration declined in most marine areas especially the Yellow Sea in which the main routes are not included in the CECA before 2020. However,



the concentration increased along coastal Zhejiang, and the highest value in the model domain rebounded
 485 to $8.3 \mu\text{g m}^{-3}$, which was in accord with the patterns of the SO_2 and NO_2 concentrations from shipping.
 This result was likely due to the recovery of fishing activities after the COVID-19 lockdown. In April
 2021, ship emissions were more evenly distributed, and hence the concentration of shipping-related $\text{PM}_{2.5}$
 only presented relatively high values in a city level, with the maximum of $4.5 \mu\text{g m}^{-3}$ in coastal Zhejiang.



490

Figure 8. Interannual variations of the potential impacts of ship emissions on $\text{PM}_{2.5}$ ($\text{PM}_{2.5_ship}$) concentrations as well as the simulated monthly average wind fields in April of (a) 2017, (b) 2018, (c) 2019, (d) 2020, and (e) 2021.

3.4.2 Trace elements (V and Ni)

V and Ni are strongly correlated with SO_2 among the chemical species emitted by ships, and thus their
 495 concentrations from shipping share similar spatial patterns. In the CMAQ model, V and Ni do not
 participate in any chemical reactions, while SO_2 can be oxidized to sulfuric acid (H_2SO_4) and sulfate.
 Therefore, emissions and meteorology are the factors affecting the concentrations of $\text{PM}_{2.5}$ -bound V and
 Ni from shipping. In 2017, the areas with the V concentration from shipping exceeding 0.5 ng m^{-3} covered
 most parts of eastern China, with the maximum of 24.5 ng m^{-3} (Fig. 9a). In contrast, for the land areas,

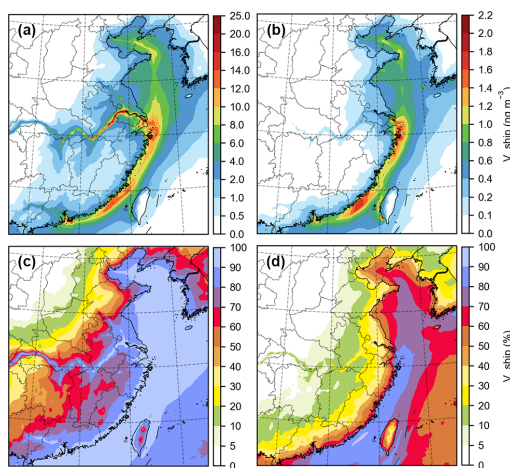


500 only coastal areas and the Yangtze River showed values over 0.1 ng m^{-3} in 2021, and the maximum along the coast substantially decreased to 2.2 ng m^{-3} (Fig. 9b). Ship emissions overwhelmingly dominated the V concentration in the marine and coastal areas as well as along the Yangtze River in 2017 (Fig. 9c). However, in 2021, the contribution of land-based emissions was closed to or even higher than that of ship emissions in the coastal areas (Fig. 9d). There was also an evident decrease in the contribution of

505 ship emissions in remote marine areas because V from land-based emissions including anthropogenic sources and mineral dust can be transported by the high-altitude westerly wind.

The spatial pattern of the Ni concentration from shipping was similar to that of the V concentration from shipping, while their relative changes from 2017 to 2021 were different (Fig. 10). The highest Ni concentration from shipping was 7.8 ng m^{-3} in 2017 and decreased to 4.1 ng m^{-3} in 2021. The V/Ni ratios in ambient particles from shipping decreased from ~ 3.0 to ~ 0.5 from 2017 to 2021. In 2017, the contribution of ship emissions to the Ni concentration was lower compared to V. Over land areas, the contour of 80% for the V concentration share generally corresponded to the contour of 40% for the Ni concentration share. It is noted that the reduction in the Ni concentration share from 2017 to 2021 was small in the model domain, and the Ni concentration share overtook the V concentration share. Despite

510 the sharp reduction in the concentrations of V and Ni from shipping, shipping is still an important source of the ambient V and Ni under the current fuel oil regulations.



520 **Figure 9.** Impacts of ship emissions on V (V_{ship}): for concentration (in ng m^{-3}) in $\text{PM}_{2.5}$ in (a) 2017 and (b) 2021; and for contribution (in %) in (c) 2017 and (d) 2021.

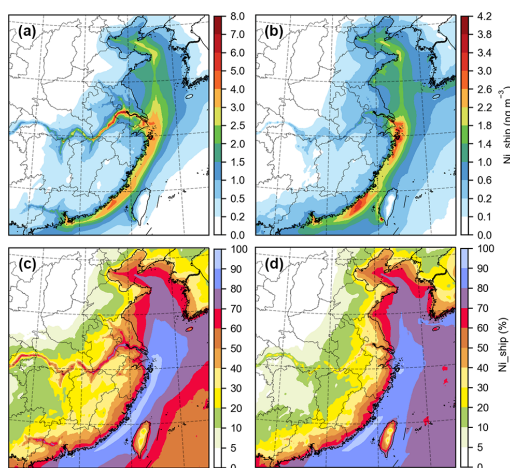


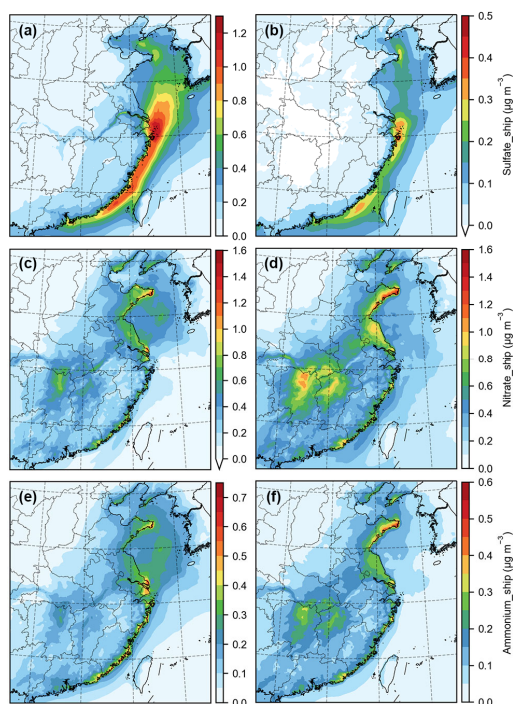
Figure 10. Impacts of ship emissions on Ni (Ni_{ship}): for concentration (in $ng\ m^{-3}$) in $PM_{2.5}$ in (a) 2017 and (b) 2021; and for contribution (in %) in (c) 2017 and (d) 2021.

525 3.4.3 Secondary inorganic aerosols

Sulfate (SO_4^{2-}), nitrate (NO_3^-), and ammonium (NH_4^+), known as SNA for short, are the most important secondary inorganic species in $PM_{2.5}$. Their concentrations are highly related to the concentrations and the conversion rates of the gas precursors including SO_2 , NO_x , and NH_3 . For the formation of sulfate, the main atmospheric oxidant is hydroxyl radical (OH) which transforms SO_2 to H_2SO_4 . Then, H_2SO_4 is neutralized by NH_3 forming $(NH_4)_2SO_4$, or dissolves in aerosol liquid water and binds with positive ions like Na^+ , leading to the higher shipping-related SO_4^{2-} concentration from the southern Yellow Sea to coastal Fujian in 2017 (Fig. 11a). The maximum of $1.2\ \mu g\ m^{-3}$ was located in the waters of Zhoushan Islands. Taking Zhoushan as an example, we found that primary sulfate emitted by ships played a minor role and secondary sulfate accounted for 91.8% of the shipping-related sulfate. As EC is a stable species, the primary sulfate concentration from shipping can be calculated through multiplying the EC concentration from shipping by the ratio of SO_4^{2-} to EC in ship-emitted PM in Table S3. Thus, the secondary part of shipping-related sulfate equals the difference of the total concentration and the primary part. Although the SO_2 concentration from shipping was also at a relatively high level along the Yangtze River, the shipping-related SO_4^{2-} concentration was significantly lower compared to the values in sea areas, which was attributed to the competitive mechanism by land-based emissions. In 2021, the shipping-related SO_4^{2-} concentration decreased with the reduction in SO_2 emissions, with the maximum of $0.46\ \mu g\ m^{-3}$. There were unexpected negative values over land areas, which was likely due to the



depletion of oxidants to generate nitric acid (HNO_3) in areas characterized by high- NO_x conditions.



545

Figure 11. Potential impacts of ship emissions on sulfate (Sulfate_{ship}), nitrate (Nitrate_{ship}), and ammonium (Ammonium_{ship}): for sulfate in (a) 2017 and (b) 2021; for nitrate in (c) 2017 and (d) 2021; and for ammonium in (e) 2017 and (f) 2021.

Most of initially emitted NO_x is in the form of NO , and is rapidly oxidized to NO_2 . During the daytime, NO_2 can be converted to HNO_3 by reacting with OH radicals. During the nighttime, NO_2 combines with NO_3 radicals originating from the oxidization of NO_2 by O_3 to generate dinitrogen pentoxide (N_2O_5). HNO_3 is formed via the reaction of N_2O_5 and water. Compared to HNO_3 , NH_3 preferentially reacts with H_2SO_4 because $(\text{NH}_4)_2\text{SO}_4$ is more stable than NH_4NO_3 . Therefore, the formation of particulate nitrate requires sufficient amount of NH_3 . The differences in the formation mechanisms between sulfate and nitrate can explain the significant differences in the spatial patterns of the concentrations between SO_4^{2-} and NO_3^- related to ship emissions. The shipping-related NH_4NO_3 in the marine atmosphere came from NH_3 transported from land areas or the transport of NH_4NO_3 already formed in coastal areas. In marine areas, the concentration of shipping-related NO_3^- only displayed moderate levels over the Yellow Sea in 2017. In comparison, higher concentration levels were concentrated along the coast, with the maximum

550

555



560 of $1.4 \mu\text{g m}^{-3}$ (Fig. 11c). In 2021, the values increased over land areas with the increase in NO_x emissions and the decrease in SO_2 emissions from shipping, while the maximum slightly increased to $1.5 \mu\text{g m}^{-3}$ located along the coast of Shandong (Fig. 11d). There was a noticeable increase in the central Yangtze River Basin, corresponding to the negative values of shipping-related SO_4^{2-} . In this study, there was no marked negative value of shipping-related NO_3^- in the model domain, which differed from the result in 565 the Mediterranean Sea also based on the CMAQ model (Fink et al., 2023a). This was caused by the huge amounts of NH_3 emissions from agriculture in China, providing an ammonia-rich condition to generate NH_4NO_3 .

The spatial patterns of shipping-related NH_4^+ were similar with those of shipping-related NO_3^- both in 2017 and 2021 (Fig. 11e and Fig. 11f). This result implied that the relatively high levels of shipping-related SO_4^{2-} in ammonia-poor offshore areas tended to present in the form of metal salt like Na_2SO_4 rather than $(\text{NH}_4)_2\text{SO}_4$. Compared to SO_4^{2-} and NO_3^- , the concentration of shipping-related NH_4^+ was at 570 a lower level due to the much smaller molar mass, with the maxima of $0.73 \mu\text{g m}^{-3}$ in 2017 and $0.58 \mu\text{g m}^{-3}$ in 2021. Overall, higher levels of potential impacts of ship emissions on SO_4^{2-} occurred in marine areas, while in land areas for NO_3^- and NH_4^+ . Given that $\text{PM}_{2.5}$ especially secondary species like nitrate 575 was underestimated in China's coastal cities in this study as discussed in Sect. 3.2, the simulated concentrations of SNA related to ship emissions were conservative.

3.4.4 Organic aerosols

Organic aerosol (OA) is categorized into primary organic aerosol (POA) and secondary organic aerosol (SOA). POA is calculated as the sum of particulate organic carbon (POC) and particulate non-carbon 580 organic matter (PNCOM), two species in the AERO7 module. POA and EC share similar atmospheric processes in the CMAQ model. In this study, the sum of the contributions of POC and PNCOM to primary $\text{PM}_{2.5}$ emitted by ships using HSFO was set to 70.8%, while this value was reduced to 33.4% in the case of burning LSFO (Table S3). Thus, the reduction in the POA concentration from shipping due to the fuel type change was more significant than those in the primary $\text{PM}_{2.5}$ concentration from shipping and also 585 the total shipping-related $\text{PM}_{2.5}$ concentration. The maximum value decreased from $0.41 \mu\text{g m}^{-3}$ in 2017 to $0.12 \mu\text{g m}^{-3}$ in 2021 (Fig. S7). The contribution of ship emissions to the ambient POA concentration showed higher values compare to the $\text{PM}_{2.5}$ concentration share, with the maximum of 41.9% in 2017 and 29.4% in 2021. The transport of secondary aerosols related to land-based emissions as well as the



restricted secondary aerosol formation in marine areas with the NH_3 -poor conditions led to lower values
590 of the $\text{PM}_{2.5}$ concentration share.

SOA, a kind of photochemical product, is produced via the reactions of VOCs or semi-volatile organic
compounds (SVOCs) with atmospheric oxidants. As discussed in Sect. 3.2, this study showed the
potential impacts of ship emissions on atmospheric photochemistry by using the zero-out method, which
differed from the situations of the real-world atmosphere such as the chemical processes in a single ship
595 plume. The potential impacts of ship emissions on the SOA and SO_4^{2-} concentrations shared similar
spatial patterns in 2017, with the maximum of $1.3 \mu\text{g m}^{-3}$ over the waters of Zhoushan Islands (Fig. 12a).
No negative value was found in the entire model domain. However, in 2021, the marine and coastal areas
displayed positive values with the maximum of $0.33 \mu\text{g m}^{-3}$ near the eastern coast of the Pearl River
Delta, whereas negative values were obtained in the central Yangtze River Basin with the minimum of -
600 $0.33 \mu\text{g m}^{-3}$ (Fig. 12b).

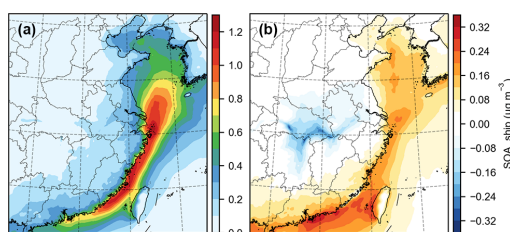


Figure 12. Potential impacts of ship emissions on secondary organic aerosols (SOA_{ship}) in (a) 2017 and (b) 2021.

For the seasonal patterns of the shipping-related SOA concentration shown in Fig. S8, the highest level
605 in the eastern offshore areas of China was found in the summer of both 2017 and 2021. In summer, high
temperature and good lighting conditions are in favor of BVOC emissions and photochemical reactions,
resulting in abundant oxidants in the background atmosphere to generate O_3 and SOA. Ship emissions
could increase the concentrations of O_3 and SOA in the NO_x -limited marine atmosphere with low NO_x
concentration. Although the NO_x and VOCs emissions from shipping increased from 2017 to 2021, the
610 shipping-related SOA concentration during the summertime decreased. This result suggested that gas-
particle partitioning of organic matter with low to medium volatility played an important role in SOA
formation. The significant decrease in the shipping-related PM was likely to reduce the impact of gas-
particle partitioning. In contrast to the pattern in summer, the potential impact of ship emissions on SOA
showed negative values in inland areas in the winter of 2021, which was indirectly caused by the O_3



615 titration by NO_x under the VOC-limited regime. The potential impact was insignificant in the other seasons, and thus the annual mean values in central China were negative. The increasing NO_x emissions along the Yangtze River led to more depletion in oxidants over inland areas during the wintertime. The minimum shipping-related SOA concentration in winter decreased from $-0.45 \mu\text{g m}^{-3}$ in 2017 to $-1.0 \mu\text{g m}^{-3}$ in 2021.

620 **3.5 Intercomparison of the impacts over the port cities**

In Sect. 3.5, the perspective will be shifted from regional scale to urban scale. For each of the 21 port cities selected in this study, the data of the grids where populous downtown areas (instead of the ports themselves) are located was extracted for the analysis on the impacts of ship emissions. Thus, the results can reflect the role of ship emissions in the presence of large amounts of land-based emissions in urban areas.

3.5.1 Effects of the implementation of the IMO Regulation

Figure 13 shows the absolute and relative impacts of ship emissions on multiple species such as SO_2 , NO_2 , $\text{PM}_{2.5}$, SO_4^{2-} , NO_3^- , NH_4^+ , carbonaceous aerosol (CA, referred to the sum of OA and EC), V, and Ni at the annual average level in China's main port cities in 2017 and 2021. On average across all the concerned cities, the SO_2 concentration from shipping reduced from $1.3 \mu\text{g m}^{-3}$ in 2017 to $0.48 \mu\text{g m}^{-3}$ in 2021 due to the implementation of the IMO Regulation. Its reduction rate was 63.3%, closed to the reduction rate of SO_2 emissions from shipping in the CECA and inland areas of China (68.4%). The share of the SO_2 concentration from shipping was 14.3% in 2017 and decreased to 9.0% in 2021. However, the NO_2 concentration from shipping increased from $4.3 \mu\text{g m}^{-3}$ to $7.1 \mu\text{g m}^{-3}$ due to the growth in shipping activities. The minima of the SO_2 and NO_2 concentrations from shipping were both observed in Qinzhou. The increase rate (65.9%) was higher than that of NO_x emissions from shipping (51.8%), because ship emissions increased the atmospheric oxidation capacity in offshore areas and more NO could be oxidized to NO_2 . The share of the NO_2 concentration from shipping rose from 13.9% to 22.6%.

The shipping-related $\text{PM}_{2.5}$ concentration reduced from $1.6 \mu\text{g m}^{-3}$ to $1.1 \mu\text{g m}^{-3}$, and the reduction rate (32.7%) was very closed to that of $\text{PM}_{2.5}$ emissions from shipping (32.8%). The shipping-related $\text{PM}_{2.5}$ concentrations in the city level ranged from $0.84 \mu\text{g m}^{-3}$ in Qinzhou to $2.7 \mu\text{g m}^{-3}$ in Zhoushan in 2017, while from $0.63 \mu\text{g m}^{-3}$ in Yingkou to $1.6 \mu\text{g m}^{-3}$ in Qingdao in 2021. It is noted that only Qinzhou



experienced an increase, though very small ($0.04 \mu\text{g m}^{-3}$), which was corresponding to the intense growth in cargo throughput of the Beibu Gulf ports approaching 100% in the past six years. After the operation of the Pinglu Canal at the end of 2026, there is still great potential for the growth in shipping activities and thus the impacts of ship emissions on the air quality in Qinzhou will be much more significant if the current policies do not change. Compared to SO_2 and NO_2 , the contribution of ship emissions to the total $\text{PM}_{2.5}$ concentration only showed a slight change from 6.8% to 5.5%. The shipping-related $\text{PM}_{2.5}$ shares in the city level ranged from 3.0% in Yingkou to 17.4% in Zhoushan in 2017, while from 2.5% in Nanjing to 10.3% in Zhoushan in 2021. Unexpectedly, they showed slight increases in five cities adjacent to the Yellow Sea including Dalian, Yantai, Qingdao, Rizhao, and Lianyungang, which was in accord with the increase in the shipping-related NO_3^- and NH_4^+ concentration shares.

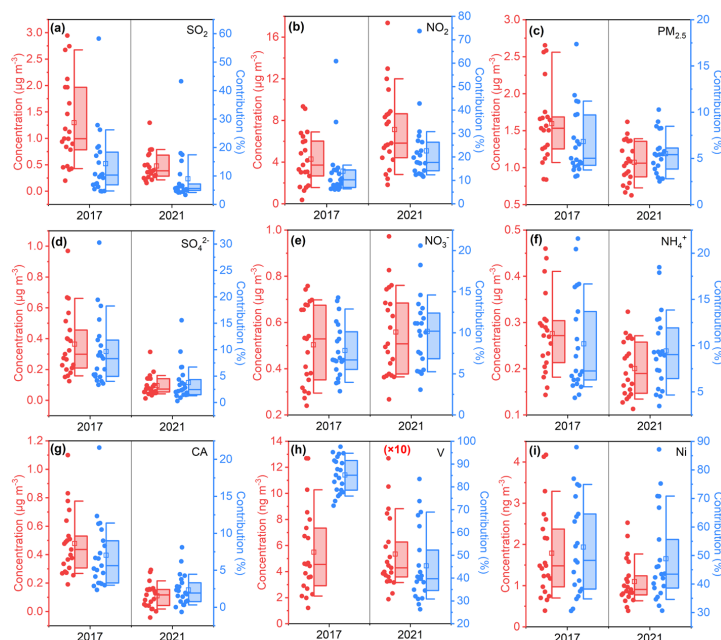


Figure 13. Impacts of ship emissions on (a) SO_2 , (b) NO_2 , (c) $\text{PM}_{2.5}$, (d) SO_4^{2-} , (e) NO_3^- , (f) NH_4^+ , (g) carbonaceous aerosol (CA), (h) V, and (i) Ni over the representative port cities of China in 2017 and 2021. Left axis and right axis show concentration and contribution, respectively. Box plots show the mean (square), median (-), lower and upper quartile (boxes), and the 10th and the 90th percentiles (whiskers) of the simulated results. The V concentration in 2021 is multiplied by 10.

For the chemical species in the shipping-related $\text{PM}_{2.5}$, the SO_4^{2-} concentration reduced from $0.36 \mu\text{g m}^{-3}$ to $0.09 \mu\text{g m}^{-3}$, with the reduction rate of 74.0%, higher than that of the SO_2 concentration from



shipping. In contrast, the shipping-related NO_3^- concentration increased by 11.0% from $0.50 \mu\text{g m}^{-3}$ to $0.56 \mu\text{g m}^{-3}$. Nevertheless, its increase rate was much smaller than that of the NO_2 concentration from shipping, indicating a low nitrogen oxidation rate (NOR). Besides the increase in the NO_x emissions from shipping, the decrease in SO_2 provided more opportunities for the neutralization of HNO_3 by NH_3 to form NH_4NO_3 . The weakened sulfate formation was demonstrated by the decrease in the contribution of the secondary SO_4^{2-} to the total SO_4^{2-} related to shipping from 89.8% to 83.9%. Because the decrease in SO_4^{2-} was more significant than the increase in NO_3^- , the shipping-related NH_4^+ concentration decreased by 27.5% from $0.28 \mu\text{g m}^{-3}$ to $0.20 \mu\text{g m}^{-3}$. The shipping-related CA concentration decreased from $0.48 \mu\text{g m}^{-3}$ to $0.11 \mu\text{g m}^{-3}$, with a reduction rate of 76.9%, even higher than that of SO_4^{2-} . The V concentration from shipping sharply dropped from 5.5 ng m^{-3} to 0.53 ng m^{-3} . In comparison, the Ni concentration from shipping decreased moderately from 1.8 ng m^{-3} to 1.1 ng m^{-3} . The reduction rates of the V and Ni concentrations from shipping were 90.3% and 38.4% respectively, closed to the reduction rates of the emissions of V (90.8%) and Ni (42.0%) from shipping. In addition, the relative impacts of ship emissions on the concentrations of SO_4^{2-} , NO_3^- , NH_4^+ , CA, V, and Ni were 9.6%, 7.9%, 10.2%, 7.0%, 85.2%, and 52.9% in 2017 and 3.8%, 10.2%, 9.4%, 2.4%, 45.4%, and 48.9% in 2021, respectively. Among the six species, only NO_3^- exhibited an increasing trend in the relative impact.

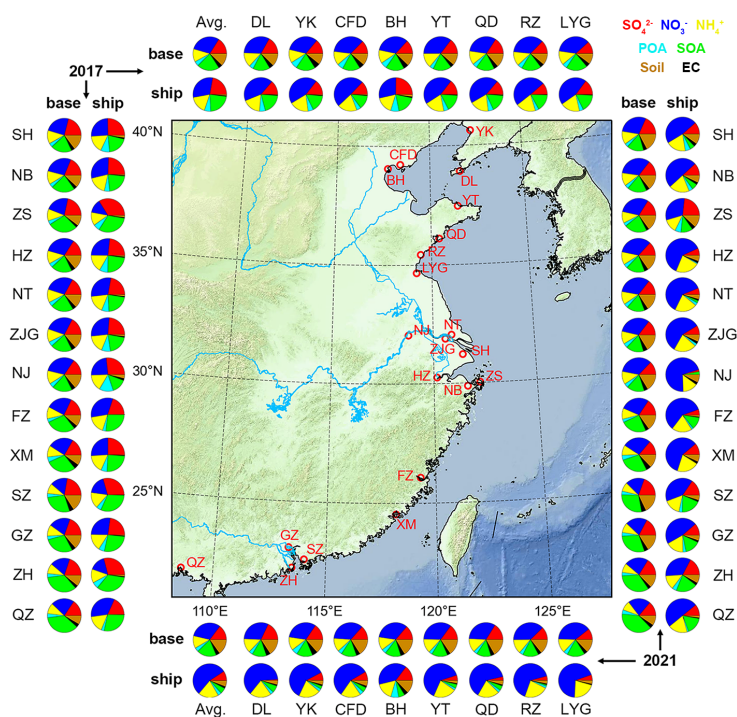
Figure 14 presents the simulated chemical speciation of $\text{PM}_{2.5}$ from all sectors and shipping over China's main port cities in 2017 and 2021. Six categories of chemical species contributing more than 95% to $\text{PM}_{2.5}$ were considered which include SO_4^{2-} , NO_3^- , NH_4^+ , POA, SOA, and Soil. Soil, a variable in the CMAQ model output, is calculated following Eq. (1):

$$\text{Soil} = 2.20 \times \text{Al} + 3.48 \times \text{Si} + 1.63 \times \text{Ca} + 2.42 \times \text{Fe} + 1.94 \times \text{Ti} \quad (1)$$

The change in the characteristics of the shipping related $\text{PM}_{2.5}$ components was far more significant compared to the $\text{PM}_{2.5}$ derived by the base runs. SO_4^{2-} accounted for 21.0% in the shipping-related $\text{PM}_{2.5}$ averaged for the concerned port cities in 2017 and decreased to 8.9% in 2021, while the percentage of SO_4^{2-} in the $\text{PM}_{2.5}$ from all sectors only decreased from 16.1% to 14.7%. This result is regarded as the potential impact and does not suggest that ship-emitted $\text{PM}_{2.5}$ contains less sulfate content than $\text{PM}_{2.5}$ from land-based sources. In the low-sulfur era, ship emissions tend to enhance the nitrate formation in the high- HNO_3 and high- NH_3 but low- H_2SO_4 conditions in China's coastal cities. Accordingly, NO_3^- has become the major component of the shipping-related $\text{PM}_{2.5}$, with the average NO_3^- share increased from 30.7% to 54.6%. The NH_4^+ share also showed an increasing trend from 17.0% to 19.6% as the decrease



in SO_4^{2-} cannot offset the increase in NO_3^- . In contrast, in the $\text{PM}_{2.5}$ from all sectors, the NO_3^- share slightly increased from 29.5% to 31.6%, while the NH_4^+ share changed little from 12.5% to 12.1%. The sum of SNA share in the shipping-related $\text{PM}_{2.5}$ rose from 69.7% to 83.5%, whereas that in the $\text{PM}_{2.5}$ from all sectors remained at the same level of ~58%. The $\text{PM}_{2.5}$ pollution from shipping which coastal urban areas suffer is mainly caused by the transport and aging processes of pollutants emitted by ships in the atmosphere from water to land, which can explain the higher SNA share in the shipping-related $\text{PM}_{2.5}$.



700

Figure 14. Simulated chemical speciation of $\text{PM}_{2.5}$ from all sectors (base) and shipping (ship) over the representative main port cities of China in 2017 (left and top) and 2021 (right and bottom). Avg. denotes the annual average. DL, YK, CFD, BH, YT, QD, RZ, LYG, SH, NB, ZS, HZ, NT, ZJG, NJ, FZ, XM, SZ, GZ, ZH, and QZ are the abbreviations of Dalian, Yingkou, Caofeidian, Binhai, Yantai, Qingdao, Rizhao, Lianyungang, Shanghai, Ningbo, Zhoushan, Hangzhou, Nantong, Zhangjiagang, Nanjing, Fuzhou, Xiamen, Shenzhen, Guangzhou, Zhuhai, and Qinzhou, respectively. The cities in the northern region are placed at the top and bottom, while the cities in the southern region are placed on the left and right.

705

Regarding the shipping-related $\text{PM}_{2.5}$, the reduction in primary $\text{PM}_{2.5}$ emissions made SNA more important, with the total SNA share rising from 69.7% to 83.4%. However, the organic aerosol share



710 decreased from 28.4% to 9.0%. The SOA share reduced from 22.2% to 5.6%, and the decrease in the
SOA share was much more significant than that in the POA share. The EC share increased from 0.8% to
1.8%, corresponding to the increase in the mapping factors of particulate EC (PEC) for ship emissions
from 4.1% to 7.0%. Due to the substantial contribution of SNA, the EC shares in the shipping-related
PM_{2.5} were significantly lower than those in the primary PM_{2.5} from shipping.

715 At the city level, both the highest NO₃⁻ and NH₄⁺ shares in the shipping-related PM_{2.5} in 2017 were
found in Rizhao corresponding to the lowest SO₄²⁻ share. However, these values were obtained in Nanjing
in the inland ultra-low sulfur control areas, with the NO₃⁻ share up to 70.7%. The SO₄²⁻ shares displayed
lower values in the northern region and higher values in the southern region, which may be partly related
to the lower aerosol acidity in the northern region (Wang et al., 2022). Zhoushan, with low NH₃ emissions,
720 showed the highest SO₄²⁻ shares both in 2017 (33.9%) and 2021 (23.2%).

3.5.2 Roles of the meteorological factors

Meteorological factors can affect both physical and chemical processes of atmospheric pollutants.
Considering the complexity of non-linear chemistry discussed above, we focused on the physical aspects
here to clarify the roles of meteorological factors on the spatiotemporal patterns of primary PM from
725 shipping in the concerned port cities. We utilized V as the tracer since V is the most convincing tracer of
ship emissions and does not participate any chemical process in the model. The impact of temporal
variations of emissions was removed because the monthly ship emissions were evenly allocated by hour
in this study. Although this simplification smoothed out the time series of the impacts of ship emissions,
it contributed to the discussion on the effects of meteorological factors such as wind patterns and the
730 PBLH. Ship emission inventories will be produced in hourly resolution based on the AIS data and used
in monthly to long-term simulations in our future work.

Figure 15 delineates the diurnal variations of the V concentration from shipping over the port cities in
every season of 2017 when ship emissions dominated the sources of ambient V. The lowest values
occurred at noon in most cases, corresponding to the highest PBLH. However, the time when the highest
735 values appeared showed significant differences by city, even by season in the same city. If the PBLH
plays a crucial role, the V concentration will simply increase with the reduction of the PBLH and reach
the peak level in early morning. This pattern was found in four cities in the YRD including Shanghai,
Hangzhou, Nantong, and Zhangjiagang in every season. A secondary peak during 20:00–21:00 was



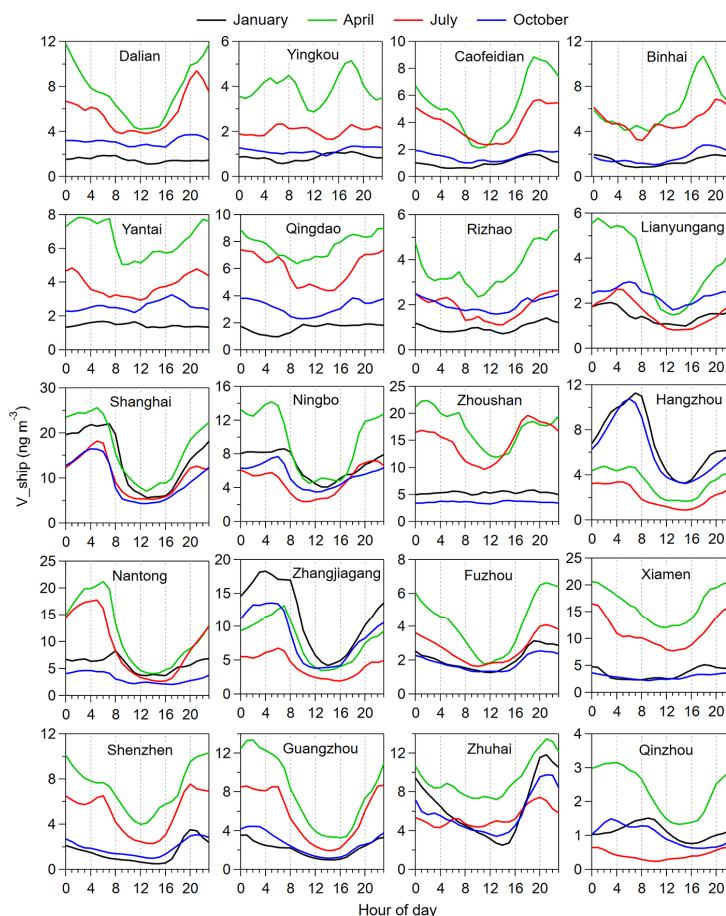
observed in Shanghai in summer, though subtle, which was caused by the intrusion of the sea breeze after
740 the dissipation of the daytime weak convergence (Shang et al., 2019; Zhai et al., 2023). Shanghai is more
likely to be affected by large synoptic systems, and urbanization results in a weaker land-breeze pattern;
meanwhile, the contribution of inland ship emissions is considerable in downtown Shanghai. The
simulation results confirmed the finding in our previous study conducted in Shanghai based on field
observation (Yu et al., 2021).

745 In Zhuhai, Shenzhen, and Fuzhou, the V concentrations from shipping peaked before midnight with
values significantly higher than those during early morning in every season, indicating that the sea-land
breeze circulation (SLBC) significantly affected the diurnal patterns in these cities, especially Zhuhai.
The SLBC impact in downtown Guangzhou was much weaker than that in Zhuhai and Shenzhen, which
was due to the dense inland shipping activities in Guangzhou. In Binhai, Caofeidian, and Yingkou, three
750 ports located in the Bohai Bay, the SLBC impact was significant in at least three seasons. In comparison,
the SLBC impact on the diurnal variations was smaller in Qingdao and Rizhao, two cities adjacent to the
Yellow Sea. Nevertheless, this impact was found in every season; the land-breeze could block the
transport of ship emissions from marine areas and counteract the PBL compression effect. In Dalian and
Yantai, the SLBC impact was noticeable in summer and autumn. The SLBC exerted impact in a certain
755 season such as summer in Ningbo and Zhoushan while winter in Xiamen. This study adopted the grid
resolution of 9 km and still characterized the impact of the SLBC, a type of local scale system. The results
in this study are rather different from those in a study conducted in the eastern United States with scarce
SLBC impact using the WRF-CAMx (Golbazi and Archer, 2023).

Besides, the seasonal variations of the V concentration from shipping in the port cities are also shown
760 in Fig. 15. The concentration peaked in spring for most of the cities due to the weak onshore airflows.
Shanghai, Zhoushan, Nantong, Fuzhou, and Xiamen, located along the eastern to southeastern coast
exhibited the lowest levels in autumn. The lowest levels were observed in winter for all the northern
cities affected by the prevailing northwesterly wind as well as two southern cities including Guangzhou
and Shenzhen affected by the prevailing northeasterly wind. The winter monsoon was adverse to the
765 transport of ship emissions to these cities. In the other cities, poor diffusion conditions enhanced the
wintertime concentration levels. It is of interest that cities close in distance did not always perform the
same seasonal pattern. For example, in the YRD, Ningbo and Zhoushan, adjacent to each other, showed
different seasonal patterns. The southerly winds in July were conducive to the transport of pollutants



emitted by ships in Ningbo Port to the Zhoushan Islands, whereas the northerly and northeasterly airflows
 770 in January and October had opposite effects. In the PRD, Guangzhou and Shenzhen were right located
 downwind of dense ship emissions in July when the southerly to southeasterly airflows prevailed, and
 thus the V concentration from shipping was at a relatively high level. However, for Zhuhai, located in
 the southwest of the PRE, the increase in the V concentration caused by ship emissions was the smallest
 in summer. Therefore, in addition to the airflow intensity, the relationship between areas with high ship
 775 emissions and prevailing airflow directions is an important factor affecting the seasonal pattern of the
 concentration of primary PM emitted by ships in receptor cities.



780 **Figure 15.** Simulated diurnal variations of the V concentrations from shipping (V_{ship}) over the representative port cities of China in January, April, July, and October of 2017.



4 Conclusions

To meet the requirements of the IMO Regulation, China carried out staged fuel oil policies for sea-going vessels including the DECA 1.0 and the DECA 2.0 which took into effect in 2017 and 2019, respectively. Besides, the inland emission control areas were implemented in 2019 and became more
785 stringent in 2020. It is of significance to evaluate the effects of the low sulfur fuel policies on air quality in China in the context of increasing shipping activities. We updated the ship emission inventory in China to 2021 based on the AIS data. The emissions of V and Ni from shipping were constrained by the field observational data and the results of on-board emission measurements. The WRF/CMAQ model were utilized to simulated the impacts on PM_{2.5} in China as well as its gas precursors (SO₂ and NO₂) and
790 components from 2017 to 2021 based on the zero-out method. The model reproduced the V and Ni concentrations as well as their seasonal and diurnal variations, whereas underestimated the secondary aerosol concentrations.

In the CECA and inland areas of China, the SO₂, PM_{2.5}, V and Ni emissions from shipping on monthly averages were 40.9 kt, 7.6 kt, 118.8 t, 41.6 t in 2017, and dropped to 12.9 kt, 5.1 kt, 11.0 t, and 24.1 t in
795 2021, respectively. The NO_x emissions from shipping increased by 51.8% from 2017 to 2021 due to the increase in ship activities. However, the emissions of SO₂, PM_{2.5}, V, and Ni from shipping reduced by 68.4%, 32.8%, 90.8%, and 42.0%, respectively, due to the implementation of the IMO Regulation and China's inland river emission control areas.

The SO₂ and NO₂ concentrations from shipping showed higher values along the main routes and spread
800 to both sides. The maximum SO₂ (NO₂) concentrations from shipping were 6.1 μg m⁻³ (17.9 μg m⁻³) in 2017 and 2.5 μg m⁻³ (26.0 μg m⁻³) in 2021. In most areas, the peak values occurred in spring while autumn for the valley values, which was attributed to the direction and intensity of the prevailing airflows. The shipping-related PM_{2.5} concentration displayed more uniform spatial patterns. In 2017, the areas with concentrations over 1 μg m⁻³ covered most of the Yellow and Bohai Seas and extended to the Middle
805 Yangtze River, with the maximum of 3.8 μg m⁻³ near Zhoushan Islands. In 2021, these areas shrunk to the coast and the central Yangtze River Basin in 2021, with the maximum of 2.6 μg m⁻³ in the eastern Shandong Peninsula. The seasonal patterns of the shipping-related PM_{2.5} concentration differed by region mainly due to the seasonality of secondary aerosol formation, whereas those of the contributions of ship emissions to was also affected by the East Asia Monsoon considering the impacts of land-based sources.



810 The shipping-related $PM_{2.5}$ concentration peaked in spring when the SNA formation was significant under the conditions of weak onshore airflows and abundant gas precursors. The offshore marine areas suffered from higher SOA concentration related to ship emissions in summer. The northeasterly airflows diluted the pollution caused by shipping in autumn. NH_3 was consumed by land-based emissions in prior to ship emissions in winter, leading to low shipping-related $PM_{2.5}$ concentration in winter. The springtime
815 concentrations of shipping-related $PM_{2.5}$, V, and Ni experienced staged reduction in most simulated areas from 2018 to 2021.

At the city level, the contributions of ship emissions to the $PM_{2.5}$ concentration over China's main port cities ranged from 3.0% to 17.4% in 2017 and 2.5% to 10.3% in 2021. The change rates of the concentrations of $PM_{2.5}$, SO_4^{2-} , NO_3^- , NH_4^+ , carbonaceous aerosols, V, and Ni related to ship emissions
820 were -32.7%, -74.0%, +11.0%, -27.5%, -76.9%, -90.3%, and -38.4%, respectively. NO_3^- has become the dominant species accounting for 54.6% in the shipping-related $PM_{2.5}$ after 2020, and can contribute to high levels of nocturnal $PM_{2.5}$ concentration. The increasing NO_x emissions from shipping and their potential impacts on $PM_{2.5}$ and O_3 are of concern, which calls for the expansion of the Tier III Regulation in more coastal waters worldwide. Besides, the sea-land breeze circulation played an important role in
825 the diurnal patterns of the concentration of primary particulate matter from shipping in most seaports, while a minor role was found in Shanghai and Guangzhou with large inland ship emissions. Our findings suggest that it is important to consider both transport pathways and formation mechanisms of secondary aerosols to combat the $PM_{2.5}$ pollution caused by shipping in different regions.

Data availability

830 The data derived from the ship emission model and the WRF/CMAQ model presented in this paper can be obtained from Yan Zhang (yan_zhang@fudan.edu.cn) upon request.

Author contribution

GY: investigation, methodology, software, validation, formal analysis, data curation, visualization, and writing – original draft preparation; YZ: conceptualization, investigation, supervision, methodology,
835 validation, project administration, funding acquisition, and writing – review and editing; QW: validation, data curation, and writing – review; ZH: methodology, software, and data curation; SJ: methodology,



software, and data curation; FY: data curation, funding acquisition, and writing – review; XY: writing – review and editing; CH: supervision, data curation, and writing – review and editing

Competing interests

840 The authors declare that they have no conflict of interest.

Acknowledgements

The work was supported by the National Natural Science Foundation of China (No. 42077195) and the Natural Science Foundation of Shanghai Committee of Science and Technology, China (No. 22ZR1407700).

845 References

- Agrawal, H., Welch, W. A., Miller, J. W., and Cocker, D. R.: Emission Measurements from a Crude Oil Tanker at Sea, *Environmental Science & Technology*, 42, 7098-7103, <https://doi.org/10.1021/es703102y>, 2008a.
- 850 Agrawal, H., Malloy, Q. G. J., Welch, W. A., Wayne Miller, J., and Cocker, D. R.: In-use gaseous and particulate matter emissions from a modern ocean going container vessel, *Atmospheric Environment*, 42, 5504-5510, 2008b.
- Agrawal, H., Welch, W. A., Henningsen, S., Miller, J. W., and Cocker, D. R.: Emissions from main propulsion engine on container ship at sea, *Journal of Geophysical Research*, 115, <https://doi.org/10.1029/2009jd013346>, 2010.
- 855 Agrawal, H., Eden, R., Zhang, X., Fine, P. M., Katzenstein, A., Miller, J. W., Ospital, J., Teffera, S., and Cocker, D. R.: Primary Particulate Matter from Ocean-Going Engines in the Southern California Air Basin, *Environmental Science & Technology*, 43, 5398-5402, <https://doi.org/10.1021/es8035016>, 2009.
- Aksoyoglu, S., Baltensperger, U., and Prévôt, A. S. H.: Contribution of ship emissions to the concentration and deposition of air pollutants in Europe, *Atmospheric Chemistry and Physics*, 16, 1895-1906, <http://doi.org/10.5194/acp-16-1895-2016>, 2016.
- 860 Anastasopoulos, A. T., Sofowote, U. M., Hopke, P. K., Rouleau, M., Shin, T., Dheri, A., Peng, H., Kulka, R., Gibson, M. D., Farah, P. M., and Sundar, N.: Air quality in Canadian port cities after regulation of low-sulphur marine fuel in the North American Emissions Control Area, *Science of the Total Environment*, 791, 147949, <https://doi.org/10.1016/j.scitotenv.2021.147949>, 2021.
- 865 Badeke, R., Matthias, V., Karl, M., and Grawe, D.: Effects of vertical ship exhaust plume distributions on urban pollutant concentration – a sensitivity study with MITRAS v2.0 and EPISODE-CityChem v1.4, *Geoscientific Model Development*, 15, 4077-4103, <https://doi.org/10.5194/gmd-15-4077-2022>, 2022.
- Celo, V., Dabek-Zlotorzynska, E., and McCurdy, M.: Chemical characterization of exhaust emissions from selected canadian marine vessels: the case of trace metals and lanthanoids, *Environmental Science & Technology*, 49, 5220-5226, <https://doi.org/10.1021/acs.est.5b00127>, 2015.
- 870



- Ministry of Transport of the People's Republic of China: Report on China's Shipping Development in 2022 (in Chinese), 2023.
- Chosson, F., Paoli, R., and Cuenot, B.: Ship plume dispersion rates in convective boundary layers for chemistry models, *Atmospheric Chemistry and Physics*, 8, 4841-4853, <https://doi.org/10.5194/acp-8-4841-2008>, 2008.
- 875 Corbin, J. C., Mensah, A. A., Pieber, S. M., Orasche, J., Michalke, B., Zanatta, M., Czech, H., Massabo, D., Buatier de Mongeot, F., Mennucci, C., El Haddad, I., Kumar, N. K., Stengel, B., Huang, Y., Zimmermann, R., Prevot, A. S. H., and Gysel, M.: Trace Metals in Soot and PM_{2.5} from Heavy-Fuel-Oil Combustion in a Marine Engine, *Environmental Science & Technology*, 52, 6714-6722, <https://doi.org/10.1021/acs.est.8b01764>, 2018.
- 880 Dalsøren, S. B., Eide, M. S., Endresen, Ø., Mjelde, A., Gravir, G., and Isaksen, I. S. A.: Update on emissions and environmental impacts from the international fleet of ships: the contribution from major ship types and ports, *Atmospheric Chemistry and Physics*, 9, 2171-2194, <https://doi.org/10.5194/acp-9-2171-2009>, 2009.
- 885 Du, Q., Zhao, C., Zhang, M., Dong, X., Chen, Y., Liu, Z., Hu, Z., Zhang, Q., Li, Y., Yuan, R., and Miao, S.: Modeling diurnal variation of surface PM_{2.5} concentrations over East China with WRF-Chem: impacts from boundary-layer mixing and anthropogenic emission, *Atmospheric Chemistry and Physics*, 20, 2839-2863, <https://doi.org/10.5194/acp-20-2839-2020>, 2020.
- EMSA – European Maritime Safety Agency and EEA – European Environment Agency: European Maritime Transport Environmental Report 2021, <https://doi.org/10.2800/3525>, 2021.
- 890 Eyring, V., Isaksen, I. S. A., Berntsen, T., Collins, W. J., Corbett, J. J., Endresen, O., Grainger, R. G., Moldanova, J., Schlager, H., and Stevenson, D. S.: Transport impacts on atmosphere and climate: Shipping, *Atmospheric Environment*, 44, 4735-4771, <https://doi.org/10.1016/j.atmosenv.2009.04.059>, 2010.
- 895 Fan, Q., Zhang, Y., Ma, W., Ma, H., Feng, J., Yu, Q., Yang, X., Ng, S. K., Fu, Q., and Chen, L.: Spatial and Seasonal Dynamics of Ship Emissions over the Yangtze River Delta and East China Sea and Their Potential Environmental Influence, *Environmental Science & Technology*, 50, 1322-1329, <https://doi.org/10.1021/acs.est.5b03965>, 2016.
- Feng, J., Zhang, Y., Li, S., Mao, J., Patton, A. P., Zhou, Y., Ma, W., Liu, C., Kan, H., Huang, C., An, J., 900 Li, L., Shen, Y., Fu, Q., Wang, X., Liu, J., Wang, S., Ding, D., Cheng, J., Ge, W., Zhu, H., and Walker, K.: The influence of spatiality on shipping emissions, air quality and potential human exposure in the Yangtze River Delta/Shanghai, China, *Atmospheric Chemistry and Physics*, 19, 6167-6183, <https://doi.org/10.5194/acp-19-6167-2019>, 2019.
- Feng, X., Ma, Y., Lin, H., Fu, T. M., Zhang, Y., Wang, X., Zhang, A., Yuan, Y., Han, Z., Mao, J., Wang, 905 D., Zhu, L., Wu, Y., Li, Y., and Yang, X.: Impacts of Ship Emissions on Air Quality in Southern China: Opportunistic Insights from the Abrupt Emission Changes in Early 2020, *Environmental Science & Technology*, 57, 16999-17010, <https://doi.org/10.1021/acs.est.3c04155>, 2023.
- Fink, L., Karl, M., Matthias, V., Oppo, S., Kranenburg, R., Kuenen, J., Jutterström, S., Moldanova, J., Majamäki, E., and Jalkanen, J.-P.: A multimodel evaluation of the potential impact of shipping on particle 910 species in the Mediterranean Sea, *Atmospheric Chemistry and Physics*, 23, 10163-10189, <https://doi.org/10.5194/acp-23-10163-2023>, 2023a.
- Fink, L., Karl, M., Matthias, V., Oppo, S., Kranenburg, R., Kuenen, J., Moldanova, J., Jutterström, S., Jalkanen, J.-P., and Majamäki, E.: Potential impact of shipping on air pollution in the Mediterranean region – a multimodel evaluation: comparison of photooxidants NO₂ and O₃, *Atmospheric Chemistry*



- 915 and Physics, 23, 1825-1862, <https://doi.org/10.5194/acp-23-1825-2023>, 2023b.
- Fu, X., Chen, D., Wang, X., Li, Y., Lang, J., Zhou, Y., and Guo, X.: The impacts of ship emissions on ozone in eastern China, *Science of the Total Environment*, 903, 166252, <https://doi.org/10.1016/j.scitotenv.2023.166252>, 2023.
- 920 Golbazi, M. and Archer, C.: Impacts of maritime shipping on air pollution along the US East Coast, *Atmospheric Chemistry and Physics*, 23, 15057-15075, <https://doi.org/10.5194/acp-23-15057-2023>, 2023.
- He, L., Wang, J., Liu, Y., Zhang, Y., He, C., Yu, Q., and Ma, W.: Selection of onshore sites based on monitoring possibility evaluation of exhausts from individual ships for Yantian Port, China, *Atmospheric Environment*, 247, <https://doi.org/10.1016/j.atmosenv.2021.118187>, 2021.
- 925 Hersbach, H., Bell, B., Berrisford, P., Biavati, G., Horányi, A., Muñoz Sabater, J., Nicolas, J., Peubey, C., Radu, R., Rozum, I., Schepers, D., Simmons, A., Soci, C., Dee, D., and Thépaut, J.-N.: ERA5 hourly data on single levels from 1940 to present, Copernicus Climate Change Service (C3S) Climate Data Store (CDS) [dataset], <https://doi.org/10.24381/cds.adbb2d47> (last access: 23 March 2023), 2023.
- Huang, C., Hu, Q., Wang, H., Qiao, L., Jing, S., Wang, H., Zhou, M., Zhu, S., Ma, Y., Lou, S., Li, L., Tao, S., Li, Y., and Lou, D.: Emission factors of particulate and gaseous compounds from a large cargo vessel operated under real-world conditions, *Environmental Pollution*, 242, 667-674, <https://doi.org/10.1016/j.envpol.2018.07.036>, 2018a.
- Huang, C., Hu, Q., Li, Y., Tian, J., Ma, Y., Zhao, Y., Feng, J., An, J., Qiao, L., Wang, H., Jing, S., Huang, D., Lou, S., Zhou, M., Zhu, S., Tao, S., and Li, L.: Intermediate Volatility Organic Compound Emissions from a Large Cargo Vessel Operated under Real-World Conditions, *Environmental Science & Technology*, 52, 12934-12942, <https://doi.org/10.1021/acs.est.8b04418>, 2018b.
- 935 IMO – International Maritime Organization: Fourth IMO GHG Study 2020, London, UK, 2021.
- Jang, E., Choi, S., Yoo, E., Hyun, S., and An, J.: Impact of shipping emissions regulation on urban aerosol composition changes revealed by receptor and numerical modelling, *npj Climate and Atmospheric Science*, 6, 52, <https://doi.org/10.1038/s41612-023-00364-9>, 2023.
- 940 Jiang, S., Zhang, Y., Yu, G., Han, Z., Zhao, J., Zhang, T., and Zheng, M.: Source-resolved atmospheric metal emissions, concentrations, and deposition fluxes into the East Asian seas, *Atmospheric Chemistry and Physics*, 24, 8363-8381, <https://doi.org/10.5194/acp-24-8363-2024>, 2024.
- Jonson, J. E., Gauss, M., Schulz, M., Jalkanen, J.-P., and Fagerli, H.: Effects of global ship emissions on European air pollution levels, *Atmospheric Chemistry and Physics*, 20, 11399-11422, <https://doi.org/10.5194/acp-20-11399-2020>, 2020.
- 945 Kang, Y., Liu, M., Song, Y., Huang, X., Yao, H., Cai, X., Zhang, H., Kang, L., Liu, X., Yan, X., He, H., Zhang, Q., Shao, M., and Zhu, T.: High-resolution ammonia emissions inventories in China from 1980 to 2012, *Atmospheric Chemistry and Physics*, 16, 2043-2058, <https://doi.org/10.5194/acp-16-2043-2016>, 2016.
- 950 Karjalainen, P., Teinila, K., Kuittinen, N., Aakko-Saksa, P., Bloss, M., Vesala, H., Pettinen, R., Saarikoski, S., Jalkanen, J. P., and Timonen, H.: Real-world particle emissions and secondary aerosol formation from a diesel oxidation catalyst and scrubber equipped ship operating with two fuels in a SECA area, *Environmental Pollution*, 292, 118278, <https://doi.org/10.1016/j.envpol.2021.118278>, 2022.
- 955 Kotchenruther, R. A.: The effects of marine vessel fuel sulfur regulations on ambient PM_{2.5} along the west coast of the U.S, *Atmospheric Environment*, 103, 121-128, <https://doi.org/10.1016/j.atmosenv.2014.12.040>, 2015.
- Kotchenruther, R. A.: The effects of marine vessel fuel sulfur regulations on ambient PM_{2.5} at coastal and



- near coastal monitoring sites in the U.S, *Atmospheric Environment*, 151, 52-61,
960 <https://doi.org/10.1016/j.atmosenv.2016.12.012>, 2017.
- Lack, D. A., Corbett, J. J., Onasch, T., Lerner, B., Massoli, P., Quinn, P. K., Bates, T. S., Covert, D. S.,
Coffman, D., Sierau, B., Herndon, S., Allan, J., Baynard, T., Lovejoy, E., Ravishankara, A. R., and
Williams, E.: Particulate emissions from commercial shipping: Chemical, physical, and optical properties,
Journal of Geophysical Research, 114, <https://doi.org/10.1029/2008jd011300>, 2009.
- 965 Lansø, A. S., Winther, M., Jensen, S. S., and Løfstrøm, P.: Impact on air quality from increasing cruise
ship activity in Copenhagen port, *Environmental Research Communications*, 5,
<https://doi.org/10.1088/2515-7620/acb90c>, 2023.
- Li, M., Zhang, Q., Kurokawa, J.-i., Woo, J.-H., He, K., Lu, Z., Ohara, T., Song, Y., Streets, D. G.,
Carmichael, G. R., Cheng, Y., Hong, C., Huo, H., Jiang, X., Kang, S., Liu, F., Su, H., and Zheng, B.:
970 MIX: a mosaic Asian anthropogenic emission inventory under the international collaboration framework
of the MICS-Asia and HTAP, *Atmospheric Chemistry and Physics*, 17, 935-963,
<https://doi.org/10.5194/acp-17-935-2017>, 2017.
- Liu, H., Jin, X., Wu, L., Wang, X., Fu, M., Lv, Z., Morawska, L., Huang, F., and He, K.: The impact of
marine shipping and its DECA control on air quality in the Pearl River Delta, China, *Science of the Total*
975 *Environment*, 625, 1476-1485, <https://doi.org/10.1016/j.scitotenv.2018.01.033>, 2018a.
- Liu, Y., Xing, J., Wang, S., Fu, X., and Zheng, H.: Source-specific speciation profiles of PM_{2.5} for heavy
metals and their anthropogenic emissions in China, *Environmental Pollution*, 239, 544-553,
<https://doi.org/10.1016/j.envpol.2018.04.047>, 2018b.
- Liu, Y., Zhang, W., Bai, Z., Yang, W., Zhao, X., Han, B., and Wang, X.: China Source Profile Shared
980 Service (CSPSS): The Chinese PM_{2.5} Database for Source Profiles, Aerosol and Air Quality Research,
17, 1501-1514, <https://doi.org/10.4209/aaqr.2016.10.0469>, 2017a.
- Liu, Z., Lu, X., Feng, J., Fan, Q., Zhang, Y., and Yang, X.: Influence of Ship Emissions on Urban Air
Quality: A Comprehensive Study Using Highly Time-Resolved Online Measurements and Numerical
Simulation in Shanghai, *Environmental Science & Technology*, 51, 202-211,
985 <https://doi.org/10.1021/acs.est.6b03834>, 2017b.
- Lv, Z., Liu, H., Ying, Q., Fu, M., Meng, Z., Wang, Y., Wei, W., Gong, H., and He, K.: Impacts of shipping
emissions on PM_{2.5} pollution in China, *Atmospheric Chemistry and Physics*, 18, 15811-15824,
<https://doi.org/10.5194/acp-18-15811-2018>, 2018.
- Ma, M., Gao, Y., Ding, A., Su, H., Liao, H., Wang, S., Wang, X., Zhao, B., Zhang, S., Fu, P., Guenther,
990 A. B., Wang, M., Li, S., Chu, B., Yao, X., and Gao, H.: Development and Assessment of a High-
Resolution Biogenic Emission Inventory from Urban Green Spaces in China, *Environmental Science &
Technology*, 56, 175-184, <https://doi.org/10.1021/acs.est.1c06170>, 2022.
- Moldanová, J., Fridell, E., Popovicheva, O., Demirdjian, B., Tishkova, V., Faccinetto, A., and Focsa, C.:
Characterisation of particulate matter and gaseous emissions from a large ship diesel engine, *Atmospheric*
995 *Environment*, 43, 2632-2641, <https://doi.org/10.1016/j.atmosenv.2009.02.008>, 2009.
- Moldanová, J., Fridell, E., Winnes, H., Holmin-Fridell, S., Boman, J., Jedynska, A., Tishkova, V.,
Demirdjian, B., Joulie, S., Bladt, H., Ivleva, N. P., and Niessner, R.: Physical and chemical
characterisation of PM emissions from two ships operating in European Emission Control Areas,
Atmospheric Measurement Techniques, 6, 3577-3596, <https://doi.org/10.5194/amt-6-3577-2013>, 2013.
- 1000 Seinfeld, J. H. and Pandis, S. N.: *Atmospheric chemistry and physics: from air pollution to climate
change*, 3rd Edition, John Wiley & Sons, 2016.
- Shang, F., Chen, D., Guo, X., Lang, J., Zhou, Y., Li, Y., and Fu, X.: Impact of Sea Breeze Circulation on



- the Transport of Ship Emissions in Tangshan Port, China, *Atmosphere*, 10, <https://doi.org/10.3390/atmos10110723>, 2019.
- 1005 Sindelarova, K., Markova, J., Simpson, D., Huszar, P., Karlicky, J., Darras, S., and Granier, C.: Copernicus Atmosphere Monitoring Service Global Biogenic VOC emissions version 3.1 (CAMSGLOB-BIOv3.1) [dataset], <https://permalink.aeris-data.fr/CAMS-GLOB-BIO> (last access: 2023/7/27), 2021.
- 1010 Spada, N. J., Cheng, X., White, W. H., and Hyslop, N. P.: Decreasing Vanadium Footprint of Bunker Fuel Emissions, *Environmental Science & Technology*, 52, 11528-11534, <https://doi.org/10.1021/acs.est.8b02942>, 2018.
- Sun, J., Qin, M., Xie, X., Fu, W., Qin, Y., Sheng, L., Li, L., Li, J., Sulaymon, I. D., Jiang, L., Huang, L., Yu, X., and Hu, J.: Seasonal modeling analysis of nitrate formation pathways in Yangtze River Delta region, China, *Atmospheric Chemistry and Physics*, 22, 12629-12646, <https://doi.org/10.5194/acp-22-12629-2022>, 2022.
- 1015 Tang, L., Ramacher, M. O. P., Moldanová, J., Matthias, V., Karl, M., Johansson, L., Jalkanen, J.-P., Yaramenka, K., Aulinger, A., and Gustafsson, M.: The impact of ship emissions on air quality and human health in the Gothenburg area – Part 1: 2012 emissions, *Atmospheric Chemistry and Physics*, 20, 7509-7530, <https://doi.org/10.5194/acp-20-7509-2020>, 2020.
- 1020 Tao, L., Fairley, D., Kleeman, M. J., and Harley, R. A.: Effects of switching to lower sulfur marine fuel oil on air quality in the San Francisco Bay area, *Environmental Science & Technology*, 47, 10171-10178, <https://doi.org/10.1021/es401049x>, 2013.
- UNCTAD – United Nations Conference on Trade and Development: Review of Maritime Transport 2023: Towards a Green and Just Transition, United Nations Publications, ISBN: 978-992-971-002886-002888, 2023.
- 1025 Viana, M., Hammingh, P., Colette, A., Querol, X., Degraeuwe, B., Vliieger, I. d., and van Aardenne, J.: Impact of maritime transport emissions on coastal air quality in Europe, *Atmospheric Environment*, 90, 96-105, <https://doi.org/10.1016/j.atmosenv.2014.03.046>, 2014.
- 1030 Wang, G., Tao, Y., Chen, J., Liu, C., Qin, X., Li, H., Yun, L., Zhang, M., Zheng, H., Gui, H., Liu, J., Huo, J., Fu, Q., Deng, C., and Huang, K.: Quantitative Decomposition of Influencing Factors to Aerosol pH Variation over the Coasts of the South China Sea, East China Sea, and Bohai Sea, *Environmental Science & Technology Letters*, 9, 815-821, <https://doi.org/10.1021/acs.estlett.2c00527>, 2022.
- 1035 Wang, X., Shen, Y., Lin, Y., Pan, J., Zhang, Y., Louie, P. K. K., Li, M., and Fu, Q.: Atmospheric pollution from ships and its impact on local air quality at a port site in Shanghai, *Atmospheric Chemistry and Physics*, 19, 6315-6330, <https://doi.org/10.5194/acp-19-6315-2019>, 2019.
- Wang, X., Yi, W., Lv, Z., Deng, F., Zheng, S., Xu, H., Zhao, J., Liu, H., and He, K.: Ship emissions around China under gradually promoted control policies from 2016 to 2019, *Atmospheric Chemistry and Physics*, 21, 13835-13853, <https://doi.org/10.5194/acp-21-13835-2021>, 2021.
- 1040 WHO – World Health Organization: Air Quality Guidelines - Update 2021, WHO Regional Office for Europe, Copenhagen, Denmark, 2021.
- Xie, X., Hu, J., Qin, M., Guo, S., Hu, M., Wang, H., Lou, S., Li, J., Sun, J., Li, X., Sheng, L., Zhu, J., Chen, G., Yin, J., Fu, W., Huang, C., and Zhang, Y.: Modeling particulate nitrate in China: Current findings and future directions, *Environment International*, 166, 107369, <https://doi.org/10.1016/j.envint.2022.107369>, 2022.
- 1045 Yang, L., Zhang, Q., Zhang, Y., Lv, Z., Wu, L., and Mao, H.: Real-world emission characteristics of an ocean-going vessel through long sailing measurement, *Science of the Total Environment*, 810, 152276,



- <https://doi.org/10.1016/j.scitotenv.2021.152276>, 2022.
- 1050 Yu, G., Zhang, Y., Yang, F., He, B., Zhang, C., Zou, Z., Yang, X., Li, N., and Chen, J.: Dynamic Ni/V Ratio in the Ship-Emitted Particles Driven by Multiphase Fuel Oil Regulations in Coastal China, *Environmental Science & Technology*, 55, 15031-15039, <https://doi.org/10.1021/acs.est.1c02612>, 2021.
- Zetterdahl, M., Moldanová, J., Pei, X., Pathak, R. K., and Demirdjian, B.: Impact of the 0.1% fuel sulfur content limit in SECA on particle and gaseous emissions from marine vessels, *Atmospheric Environment*, 145, 338-345, <https://doi.org/10.1016/j.atmosenv.2016.09.022>, 2016.
- 1055 Zhai, J., Yu, G., Zhang, J., Shi, S., Yuan, Y., Jiang, S., Xing, C., Cai, B., Zeng, Y., Wang, Y., Zhang, A., Zhang, Y., Fu, T. M., Zhu, L., Shen, H., Ye, J., Wang, C., Tao, S., Li, M., Zhang, Y., and Yang, X.: Impact of Ship Emissions on Air Quality in the Greater Bay Area in China under the Latest Global Marine Fuel Regulation, *Environmental Science & Technology*, 57, 12341-12350, <https://doi.org/10.1021/acs.est.3c03950>, 2023.
- 1060 Zhang, F., Xiao, B., Liu, Z., Zhang, Y., Tian, C., Li, R., Wu, C., Lei, Y., Zhang, S., Wan, X., Chen, Y., Han, Y., Cui, M., Huang, C., Wang, H., Chen, Y., and Wang, G.: Real-world emission characteristics of VOCs from typical cargo ships and their potential contributions to secondary organic aerosol and O₃ under low-sulfur fuel policies, *Atmospheric Chemistry and Physics*, 24, 8999-9017, <https://doi.org/10.5194/acp-24-8999-2024>, 2024.
- 1065 Zhang, X., Zhang, Y., Liu, Y., Zhao, J., Zhou, Y., Wang, X., Yang, X., Zou, Z., Zhang, C., Fu, Q., Xu, J., Gao, W., Li, N., and Chen, J.: Changes in the SO₂ Level and PM_{2.5} Components in Shanghai Driven by Implementing the Ship Emission Control Policy, *Environmental Science & Technology*, 53, 11580-11587, <https://doi.org/10.1021/acs.est.9b03315>, 2019a.
- Zhang, Y., Deng, F., Man, H., Fu, M., Lv, Z., Xiao, Q., Jin, X., Liu, S., He, K., and Liu, H.: Compliance and port air quality features with respect to ship fuel switching regulation: a field observation campaign, SEISO-Bohai, *Atmospheric Chemistry and Physics*, 19, 4899-4916, <https://doi.org/10.5194/acp-19-4899-2019>, 2019b.
- 1075 Zhao, J., Zhang, Y., Xu, H., Tao, S., Wang, R., Yu, Q., Chen, Y., Zou, Z., and Ma, W.: Trace Elements From Ocean-Going Vessels in East Asia: Vanadium and Nickel Emissions and Their Impacts on Air Quality, *Journal of Geophysical Research: Atmospheres*, 126, e2020JD033984, <https://doi.org/10.1029/2020jd033984>, 2021.
- Zhao, M., Zhang, Y., Ma, W., Fu, Q., Yang, X., Li, C., Zhou, B., Yu, Q., and Chen, L.: Characteristics and ship traffic source identification of air pollutants in China's largest port, *Atmospheric Environment*, 64, 277-286, <https://doi.org/10.1016/j.atmosenv.2012.10.007>, 2013.
- 1080 Zheng, B., Zhang, Q., Geng, G., Chen, C., Shi, Q., Cui, M., Lei, Y., and He, K.: Changes in China's anthropogenic emissions and air quality during the COVID-19 pandemic in 2020, *Earth System Science Data*, 13, 2895-2907, <https://doi.org/10.5194/essd-13-2895-2021>, 2021.
- Zheng, H., Cai, S., Wang, S., Zhao, B., Chang, X., and Hao, J.: Development of a unit-based industrial emission inventory in the Beijing–Tianjin–Hebei region and resulting improvement in air quality modeling, *Atmospheric Chemistry and Physics*, 19, 3447-3462, <https://doi.org/10.5194/acp-19-3447-2019>, 2019.